Cherenkov radiation and emission of surface polaritons from charges moving paraxially outside a dielectric cylindrical waveguide

A. A. Saharian ![ORCID],[1,2,*] L. Sh. Grigoryan,[1] A. Kh. Grigorian,[1] H. F. Khachatryan,[1] and A. S. Kotanjyan[1,2]
[1]*Institute of Applied Problems in Physics NAS RA, 25 Hr. Nersessian Street, 0014 Yerevan, Armenia*
[2]*Department of Physics, Yerevan State University, 1 Alex Manoogian Street, 0025 Yerevan, Armenia*

We investigate the radiation from a charged particle moving outside a dielectric cylinder parallel to its axis. It is assumed that the cylinder is immersed into a homogeneous medium. The expressions are given for the vector potential and for the electric and magnetic fields. The spectral distributions are studied for three types of radiation: (i) Cherenkov radiation (CR) in the exterior medium, (ii) radiation on the guided modes of the dielectric cylinder, and (iii) emission of surface polaritons. Unlike the first two types of radiation, there is no velocity threshold for the generation of surface polaritons. The corresponding radiation is present in the spectral range where the dielectric permittivities of the cylinder and surrounding medium have opposite signs. The spectral range of the emitted surface polaritons becomes narrower with decreasing energy of the particle. The general results are illustrated for a special case of the Drude model for dispersion of the dielectric permittivity of the cylinder. We show that the presence of the cylinder may lead to the appearance of strong narrow peaks in the spectral distribution of the CR in the exterior medium. The conditions are specified for the appearance of those peaks and the corresponding heights and widths are analytically estimated. The collective effects of particles in bunches are discussed.

I. INTRODUCTION

The polarization of a medium by moving charged particles gives rise to a number of radiation processes. Examples are the Cherenkov radiation (CR), transition radiation, and diffraction radiation. Among those radiation processes, the remarkable properties of the CR (for reviews see [1,2]) have resulted in a wide variety of applications, including the counting and identification of high-energy particles, cosmic-ray physics, high-power radiation sources in various spectral ranges, particle accelerating systems, medical imaging and therapy, and so on. These applications motivate the importance of further investigations for various mechanisms to control the spectral and angular characteristics of the radiation intensity. In particular, recent advances in nanophysics, photonic crystals, and metamaterials provide new possibilities for the CR manipulations. Technologies are available that allow one to design materials with specified electric and magnetic properties, including the dispersion relations for effective dielectric permittivity and magnetic permeability [3]. An exciting possibility is that the permittivity and permeability can be made simultaneously negative in some frequency range (double-negative or left-handed metamaterials). In that spectral range, the wave vector and the electromagnetic field vectors form a left-handed system and the CR is emitted in the backward direction with respect to the velocity of the charged particle (reversed CR) [4] (for reviews, see [5]). Significant progress in metamaterial-related research has stimulated active

theoretical and experimental investigations of the reversed CR (see [6,7] and references therein).

From the point of view of the CR characteristics control, another important area of research is the investigation of the influence of interfaces of media with different electrodynamical properties. Previous considerations of the effects have included planar, cylindrical, and spherical boundaries (for reviews of the early research, see [1,2]). More complicated geometries and approximate methods for evaluation of the radiation fields and intensity have been considered in [8]. The CR from a short relativistic electron bunch in dielectric loaded waveguides with different periodic structures is a promising candidate for a high-power narrow-bandwidth source with adjustable spectral range (see, for instance, [9–11] and references therein). Various amplification mechanisms have been discussed. The Cherenkov emission of surface waves in planar structures has been considered in [12]. The authors of [13] investigated the CR emitted by surface plasmon polaritons.

In the present paper, we consider the CR and the emission of guided modes and surface polaritons by charged particles moving outside a cylindrical dielectric waveguide, parallel to its axis (for various aspects of interactions of charged particles with cylindrical structures, see [14] and references given there). Exact analytical expressions are provided for the spectral distributions of all these types of radiation. The conditions are specified under which the cylinder can essentially influence the spectral density of the CR in the surrounding medium. Aside from applications as a source of the electromagnetic radiation in various spectral regions, the presented results can be used to test the accuracy of various approximate methods used for investigation of the CR in more complicated

_____
*saharian@ysu.am

geometries of interfaces. The properties of the emitted surface polaritons are highly sensitive to the geometry of the surface and this offers an alternative surface probe. Among important physical realizations of cylindrical waveguides, with radii tunable in a relatively wide range, are metallic and semiconductor carbon nanotubes.

The layout of the paper is as follows. In the next section, expressions for the vector potential and for the electric and magnetic fields are provided. Assuming that the Cherenkov condition in the exterior medium is satisfied, in Sec. III a formula is derived for the spectral density of the radiation evaluating the energy flux through a cylindrical surface with large radius. The features of the radiation intensity are described depending on the relative permittivity. The energy losses are investigated in Sec. IV. An alternative expression is provided for the spectral density of the CR in the exterior medium. The radiation on the guided modes of the dielectric cylinder is discussed in Sec. V. The radiation intensity for surface polaritons is considered in Sec. VI. Section VII concludes the main results of the paper.

II. ELECTROMAGNETIC FIELDS

Consider a point charge q moving parallel to the axis of a cylinder with dielectric permittivity ε_0 and with the radius r_c. The distance of the charge trajectory from the axis will be denoted by $r_0 > r_c$ and it will be assumed that the cylinder is immersed into a homogeneous medium with dielectric permittivity ε_1 (see Fig. 1; the magnetic permeabilities for both the cylinder and surrounding medium will be taken to be a unit). In accordance with the problem symmetry, we will use cylindrical coordinates (r, ϕ, z) with the z axis along the axis of the cylinder. In the generalized Lorentz gauge, the vector potential of the electromagnetic field created by the charge is expressed in terms of the electromagnetic field Green tensor $G_{il}(\mathbf{r}, t, \mathbf{r}', t')$ as

$$A_i(t, \mathbf{r}) = -\frac{1}{2\pi^2 c} \int dt' d\mathbf{r}' \sum_{l=1}^{3} G_{il}(t, \mathbf{r}, t', \mathbf{r}') j_l(t', \mathbf{r}'),$$
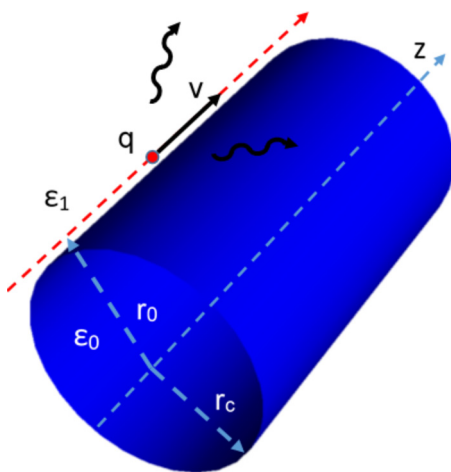
(2.1)

FIG. 1. The problem geometry and the notations.

where $j_l(t, \mathbf{r})$ is the current density for the source. In the problem under consideration, the only nonzero component of the latter is given by

$$j_3(t, \mathbf{r}) = \frac{q}{r} v \delta(r - r_0) \delta(\phi - \phi_0) \delta(z - vt),$$

(2.2)

with v being the charge velocity.

It is convenient to write the relation (2.1) in terms of the partial Fourier components $A_{l,n}(k_z, r)$ of the vector potential defined in accordance with

$$A_l(t, \mathbf{r}) = \sum_{n=-\infty}^{\infty} e^{in(\phi - \phi_0)} \int_{-\infty}^{\infty} dk_z \, e^{ik_z(z - vt)} A_{l,n}(k_z, r).$$

(2.3)

By using the Fourier expansion,

$$G_{il}(t, \mathbf{r}, t', \mathbf{r}') = \sum_{n=-\infty}^{\infty} \int_{-\infty}^{\infty} d\omega \int_{-\infty}^{\infty} dk_z \, G_{il,n}(\omega, k_z, r, r')$$

$$\times e^{in(\phi - \phi') + ik_z(z - z') - i\omega(t - t')},$$

(2.4)

from (2.1) we get

$$A_{l,n}(k_z, r) = -\frac{qv}{\pi c} G_{l3,n}(vk_z, k_z, r, r_0).$$

(2.5)

In [15], a recurrence scheme was developed for evaluation of the Green tensor in a medium with an arbitrary number of cylindrically symmetric homogeneous layers. In the problem at hand, the Green tensor is obtained by using the corresponding tensor in a homogeneous medium. In particular, for the region $r > r_0$, the Fourier components of the Green tensor appearing in (2.5) are given by the expressions [15]

$$G_{l3,n}(\omega, k_z, r, r_0) = \frac{i^{2-l} k_z}{2r_c} J_n(\lambda_0 r_c) \frac{H_n(\lambda_1 r_0)}{\alpha_n V_n^H}$$

$$\times \sum_{p=\pm 1} p^{l-1} J_{n+p}(\lambda_0 r_c) \frac{H_{n+p}(\lambda_1 r)}{V_{n+p}^H},$$

$$G_{33,n}(\omega, k_z, r, r_0) = \frac{\pi}{2i} \left[J_n(\lambda_1 r_0) - H_n(\lambda_1 r_0) \frac{V_n^J}{V_n^H} \right] H_n(\lambda_1 r),$$

(2.6)

where $l = 1, 2$, and $\lambda_j^2 = \omega^2 \varepsilon_j / c^2 - k_z^2$ with $j = 0, 1$. In (2.6), $J_n(x)$ is the Bessel function, $H_n(x) = H_n^{(1)}(x)$ is the Hankel function of the first kind, and we have introduced the notation

$$V_n^F = J_n(\lambda_0 r_c) \partial_{r_c} F_n(\lambda_1 r_c) - [\partial_{r_c} J_n(\lambda_0 r_c)] F_n(\lambda_1 r_c),$$

(2.7)

for $F = J, H$. The function α_n in the expression for the component $G_{l3,n}(\omega, k_z, r, r')$ is given by the formula

$$\alpha_n = \frac{\varepsilon_0}{\varepsilon_1 - \varepsilon_0} + \frac{1}{2} \sum_{l=\pm 1} \left[1 - \frac{\lambda_1}{\lambda_0} \frac{J_{n+l}(\lambda_0 r_c) H_n(\lambda_1 r_c)}{J_n(\lambda_0 r_c) H_{n+l}(\lambda_1 r_c)} \right]^{-1}.$$

(2.8)

The eigenmodes of the dielectric cylinder are determined from the equation $\alpha_n = 0$. They are poles of the integrand in (2.4) for the corresponding components of the Green tensor.

The Fourier components of the vector potential are given by (2.5) with the Green tensor components from (2.6), where

now $\omega = vk_z$ and λ_j is given by the expression

$$\lambda_j^2 = k_z^2(\beta_j^2 - 1), \tag{2.9}$$

with $\beta_j^2 = (v/c)^2\varepsilon_j$. In the discussion below, we will assume that the exterior medium is transparent and the permittivity ε_1 is real. Both cases $\beta_1 > 1$ and $\beta_1 < 1$ will be considered. In the second case λ_1 is purely imaginary and its sign is determined in accordance with $\lambda_1 = i|k_z|\sqrt{1-\beta_1^2}$. Note that in the arguments of the Hankel functions, only λ_1 appears and with this choice of the sign they are reduced to the Macdonald functions $K_\nu(|\lambda_1|x)$, with $x = r, r_0, r_c$. For real ε_j and $\beta_j^2 > 1$, the signs are defined in accordance with $\lambda_j = k_z\sqrt{\beta_j^2 - 1}$.

Fourier expanding the electric and magnetic fields $E_l(t, \mathbf{r})$ and $H_l(t, \mathbf{r})$, similar to (2.3), with the Fourier coefficients $E_{l,n}(k_z, r)$, $H_{l,n}(k_z, r)$, for the magnetic field one finds

$$H_{l,n}(k_z, r) = \frac{qvk_z}{4i^{l-1}c}\sum_{p=\pm 1} p^{l-1}f_n^{(p)}H_{n+p}(\lambda_1 r), \quad l = 1, 2,$$

$$H_{3,n}(k_z, r) = \frac{iqvk_z}{4c}\sqrt{\beta_1^2 - 1}\sum_{p=\pm 1} pf_n^{(p)}H_n(\lambda_1 r), \tag{2.10}$$

where, for $p = \pm 1$, we have defined the functions

$$f_n^{(p)} = -\sqrt{\beta_1^2 - 1}J_n(\lambda_1 r_0) + \frac{H_n(\lambda_1 r_0)}{V_n^H}\left[\sqrt{\beta_1^2 - 1}V_n^J + \frac{2ipk_z}{\pi}\frac{J_n(\lambda_0 r_c)}{r_c\alpha_n}\frac{J_{n+p}(\lambda_0 r_c)}{V_{n+p}^H}\right]. \tag{2.11}$$

By taking into account that for the function from (2.7) one has $V_{-n}^F = V_n^F$, $F = J, H$, it can be seen that

$$f_{-n}^{(p)} = (-1)^n f_n^{(-p)}. \tag{2.12}$$

The Fourier coefficients for the electric field are obtained from the Maxwell equations and are given by

$$E_{l,n}(k_z, r) = \frac{qk_z}{8i^l\varepsilon_1}\sum_{p=\pm 1} p^l\left[(\beta_1^2 + 1)f_n^{(p)} - (\beta_1^2 - 1)f_n^{(-p)}\right]H_{n+p}(\lambda_1 r),$$

$$E_{3,n}(k_z, r) = \frac{qk_z}{4\varepsilon_1}\sqrt{\beta_1^2 - 1}\sum_{p=\pm 1} f_n^{(p)}H_n(\lambda_1 r), \tag{2.13}$$

where $l = 1, 2$. From (2.12), we get the following relations for the Fourier components of the fields:

$$E_{l,-n}(k_z, r) = (-1)^{l+1}E_{l,n}(k_z, r), \; H_{l,-n}(k_z, r)$$
$$= (-1)^l H_{l,n}(k_z, r), \tag{2.14}$$

for $l = 1, 2, 3$. Note that we also have the relations $E_{l,-n}(-k_z, r) = E_{l,n}^*(k_z, r)$ and $H_{l,-n}(-k_z, r) = H_{l,n}^*(k_z, r)$, where the star stands for the complex conjugate.

The electromagnetic fields for a charge moving in a homogeneous medium with dielectric permittivity ε_1 are obtained from the expressions given above, taking $\varepsilon_0 = \varepsilon_1$. In this limit, $V_n^J = 0$ and $V_n^H = 2i/\pi r_c$, whereas the function α_n tends to infinity. Hence, the corresponding Fourier components are given by (2.10) and (2.13), with the replacement

$$f_n^{(p)} \to -\sqrt{\beta_1^2 - 1}J_n(\lambda_1 r_0). \tag{2.15}$$

Now we see that the fields in the exterior region are decomposed into the parts corresponding to the fields in a homogeneous medium with permittivity ε_1 and the part induced by the presence of the cylinder. The latter is given by (2.10) and (2.13), excluding the first term in the right-hand side of (2.11). The Fourier components have poles at the zeros of the function α_n. As mentioned before, those zeros determine the eigenmodes of the cylinder. The expressions for the fields in the region $r_c < r < r_0$ are obtained from the corresponding formulas in the region $r > r_0$, given above, by the replacements $J \to H$, $H \to J$ in the parts corresponding to the fields in a homogeneous medium with permittivity ε_1.

The cylinder-induced contributions are described by the same expressions for all values $r > r_1$. The fields inside the cylinder can be found by using the corresponding expressions of the Green tensor components from [15].

III. CHERENKOV RADIATION IN THE EXTERIOR MEDIUM

Having the electric and magnetic fields in the form of the Fourier expansion, we can investigate the radiation intensity emitted by the charged particle. In the problem at hand, we have three types of radiations. The first one corresponds to the CR in the exterior medium influenced by the presence of the cylinder. The second one is the radiation emitted on the guided modes of the cylinder and propagates inside the waveguide. The corresponding fields exponentially decay in the exterior medium. Under certain conditions on the characteristics of the media, one can also have the radiation in the form of surface polaritons (surface modes). We start our discussion from the radiation in the exterior medium at large distances from the cylinder, $r \gg r_c$. From the expressions (2.10) and (2.13), it follows that this kind of radiation is present under the condition $\lambda_1^2 > 0$. By taking into account the expression (2.9), the latter condition is translated to $\beta_1^2 > 1$, which is the Cherenkov condition for the exterior medium. The corresponding radiation is the CR influenced by the dielectric cylinder. For $\lambda_1^2 < 0$, the Hankel functions in (2.10) and (2.13) are expressed in terms of the Macdonald functions $K_n(|\lambda_1|r)$, $K_{n+p}(|\lambda_1|r)$, and the Fourier components exponentially decay at large distances from the cylinder, $r \gg v/\omega$.

We denote by I the energy flux per unit time through the cylindrical surface of radius r. It is given by the expression

$$I = \frac{c}{4\pi} \int_0^{2\pi} d\phi \int_{-\infty}^{\infty} dz \, r \mathbf{n} \cdot [\mathbf{E} \times \mathbf{H}], \tag{3.1}$$

where $\mathbf{n}$ is the unit normal to the integration surface. By using the Fourier expansions of the fields, we get

$$I = \pi c r \sum_{n=-\infty}^{\infty} \int_{-\infty}^{\infty} dk_z \, \mathbf{n} \cdot [\mathbf{E}_n(k_z, r) \times \mathbf{H}_n^*(k_z, r)]. \tag{3.2}$$

Under the condition $\lambda_1^2 > 0$, substituting the expressions for the Fourier components, using the relation (2.12) and the asymptotic expressions of the Hankel functions for large arguments, at large distances from the cylinder we find

$$I = \int d\omega \frac{dI}{d\omega}, \tag{3.3}$$

with the spectral density

$$\frac{dI}{d\omega} = \frac{q^2 \omega}{2v\varepsilon_1} \sum_{n=0}^{\infty}{}' \left[\left| f_n^{(1)} + f_n^{(-1)} \right|^2 + \beta_1^2 \left| f_n^{(1)} - f_n^{(-1)} \right|^2 \right], \tag{3.4}$$

where, in the expressions (2.11) for $f_n^{(\pm 1)}$, the quantities λ_j are given by (2.9) with $k_z = \omega/v$. In (3.3), the integration over ω goes over the part of the region $\omega \in [0, \infty)$, where the condition $\beta_1^2 > 1$ is obeyed and the prime under the sign of the summation in (3.4) means that the term $n = 0$ should be taken with an additional coefficient $1/2$. An alternative representation for the spectral distribution of the radiation intensity $dI/d\omega$, based on the evaluation of the energy losses, will be given below [see (4.9)]. In deriving (3.4), we have used the asymptotic expressions for the functions $H_n(\lambda_1 r)$ and $H_{n+p}(\lambda_1 r)$ in (2.10) and (2.13) that are valid in the range $\lambda_1 r \gg 1$. This corresponds to the distances from the cylinder axis that are much larger than the radiation wavelength. For a cylinder with finite length L_c, additional conditions $r \ll L_c$ and $r_c \ll L_c$ should be imposed.

From the relation $\omega = k_z v$, it follows that the radiation described by (3.4) propagates along the Cherenkov cone having the opening angle $\theta = \theta_{\mathrm{Ch}}$ with respect to the cylinder axis, where $\cos \theta_{\mathrm{Ch}} = 1/\beta_1$. In the limit $\varepsilon_0 \to \varepsilon_1$, the functions $f_n^{(p)}$ are given by the right-hand side in (2.15), and from (3.4) the Tamm-Frank formula is obtained for the CR in a homogeneous transparent medium. In the limit $r_c \to 0$ for fixed values of the other parameters, from (3.4) to the leading order, we obtain the corresponding result in a homogeneous medium. The leading contribution to the cylinder-induced part in (3.4) comes from the terms with $n = 0, 1$, and that contribution behaves as $(\omega r_c/v)^2$. The contributions of the terms with $n \geqslant 2$ behave like $(\omega r_c/v)^{2n}$. Note that the quantity $\omega^{-1} dI/d\omega$, which determines the number of the radiated quanta (see below), depends on the frequency and on the cylinder radius in the form of the product ωr_c. Hence, the limiting behavior for small r_c also determines the behavior of the radiation intensity for small frequencies. Namely, for $\omega r_c/v \ll 1$, the cylinder-induced contribution to the number of the radiated quanta behaves as ω^2 for the terms with $n = 1, 2$ and as ω^{2n} for $n \geqslant 2$.

In the figures below, we present the spectral density of the number of photons radiated per unit length of the charge trajectory:

$$\frac{d^2N}{dz d\omega} = \frac{1}{\hbar \omega v} \frac{dI}{d\omega}. \tag{3.5}$$

The corresponding quantity for the CR in a transparent homogeneous medium with permittivity ε_1 is given by

$$\frac{d^2N_0}{dz d\omega} = \frac{q^2}{\hbar c^2} \left(1 - \frac{1}{\beta_1^2} \right). \tag{3.6}$$

In Fig. 2, we display the ratio

$$R_N = \frac{d^2N/dz d\omega}{d^2N_0/dz d\omega} \tag{3.7}$$

as a function of $\omega r_c/c$ for several values of the ratio r_0/r_c (the numbers near the curves). The graphs are plotted for the electron energy $\mathcal{E}_e = 2$ MeV and for $\varepsilon_1 = 3.8$ (average value for the real part of the dielectric permittivity for a fused quartz in the frequency range $\lesssim 1$ THz; in that range, the imaginary part of the permittivity is small, $\lesssim 10^{-3}$). The left and right panels correspond to $\varepsilon_0 = 1$ and $\varepsilon_0 = 2.2$ (the real part of the dielectric permittivity for teflon).

As seen from the graphs, we have characteristic oscillations with relatively small shifts around the value corresponding to the radiation in a homogeneous medium. The oscillation frequency increases with increasing r_0/r_c. In the case corresponding to the left panel of Fig. 2, the CR inside the cylinder is absent and the oscillations are a consequence of the interference between the direct CR and radiation reflected from the cylinder. For small wavelengths, compared to the waveguide diameter, the oscillations enter the quasiperiodic regime. The beginning of that regime with respect to the radiation wavelength increases with increasing values of the ratio r_0/r_c. For small frequencies, the presence of a cylindrical hole in a homogeneous medium leads to the decrease of the radiation intensity. That is related to the fact that a part of the medium is excluded from the radiation process. For the example considered on the right panel of Fig. 2, the Cherenkov condition for the cylinder material is obeyed and the interference pattern is more complicated. It is formed by the interference of the direct radiation, the radiation reflected from the cylinder, and the CR formed inside the cylinder. We have $\varepsilon_0 < \varepsilon_1$ and, as in the previous case, here the radiation intensity for large wavelengths is smaller than that for a homogeneous medium.

For the graphs in Fig. 2 we have taken $\varepsilon_1 > \varepsilon_0$. The behavior of the radiation intensity is essentially different for $\varepsilon_1 < \varepsilon_0$. This is seen in Figs. 3 and 4, where we have plotted R_N versus $\omega r_c/c$ for $\varepsilon_0 = 3.8$, $\varepsilon_1 = 2.2$. In Fig. 3, we have taken $\mathcal{E}_e = 2$ MeV, $r_0/r_c = 1.2$ (left panel) and $r_0/r_c = 1.1$ (right panel). Figure 4 is plotted for $r_0/r_c = 1.05$ and for the energies $\mathcal{E}_e = 2$ MeV (full curve) and $\mathcal{E}_e = 10$ MeV (dashed curve). We have numerically checked that the curves corresponding to the energies $\mathcal{E}_e > 10$ MeV practically coincide with those for the energy 10 MeV. This is a consequence of the fact [also seen from the general formula (3.4)] that the effects we consider are sensitive to the velocity of the charge and not to the energy in the range $\mathcal{E}_e \gg m_e c^2$. As we see from the graphs, for the charge trajectory sufficiently close to the
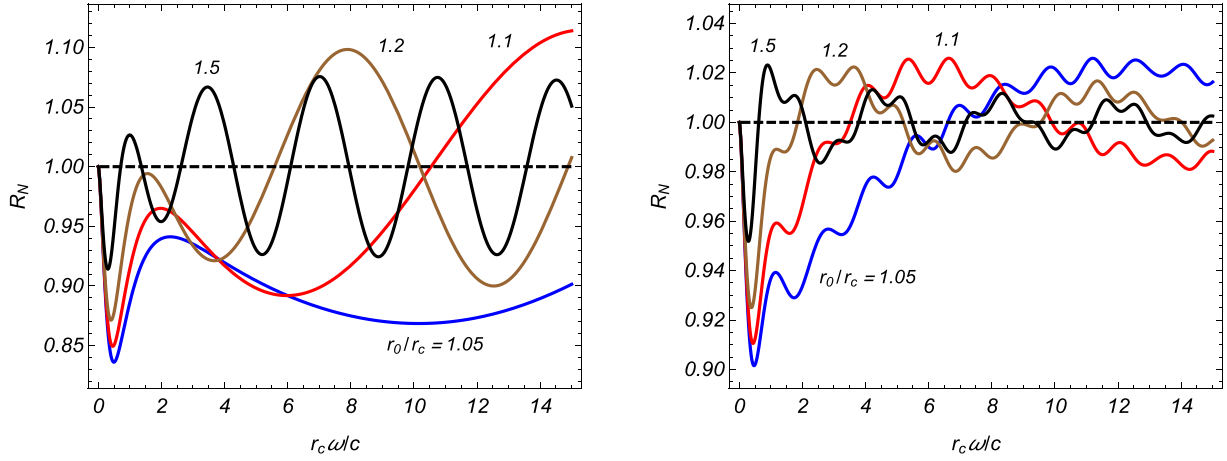
FIG. 2. The ratio R_N as a function of $\omega r_c/c$ for the electron energy $\mathcal{E}_e = 2$ MeV and for $\varepsilon_1 = 3.8$. The left and right panels correspond to $\varepsilon_0 = 1$ and $\varepsilon_0 = 2.2$ and the numbers near the curves are the values of r_0/r_c.

cylinder, strong narrow peaks appear in the spectral density of the radiation intensity. The amplification of the radiation intensity for relatively small values of $\omega r_c/c$ is related to the fact that now $\varepsilon_0 > \varepsilon_1$ and the CR inside the cylinder is more intense than in an equivalent cylinder with permittivity ε_1.

The appearance of the strong narrow peaks in the spectral distribution of the CR in the exterior medium is an interesting effect induced by the cylinder. Their presence can be understood analytically by using the formula (3.4) for the radiation intensity (see, also, the discussions in [16] and [17] for the peaks in the angular distribution of the radiation intensity from charges rotating around or inside a dielectric cylinder along circular and helical trajectories, respectively). First of all, it can be seen that the peaks come from the terms in the series on the right-hand side of (3.4) with large values of n. For large n, one has the following asymptotic expression for the Neumann function (the leading term in the Debye's asymptotic expansion; see [18]):

$$Y_n(ny) \sim \frac{2e^{n\zeta(y)}}{\sqrt{2\pi n}(1-y^2)^{1/4}}, \tag{3.8}$$

with $0 < y < 1$, and

$$\zeta(y) = \ln \frac{1+\sqrt{1-y^2}}{y} - \sqrt{1-y^2}. \tag{3.9}$$

The function (3.9) is positive and monotonically decreasing in the region $0 < y < 1$ with $\zeta(1) = 0$. For $y > 1$ and for large n, the function $Y_n(ny)$ exhibits an oscillating behavior [see the analog behavior for the function $J_n(ny)$ in (3.10) below]. For the Bessel function, one has the asymptotics [18]

$$J_n(ny) \sim \frac{e^{-n\zeta(y)}}{\sqrt{2\pi n}(1-y^2)^{1/4}}, \quad 0 < y < 1,$$

$$J_n(ny) \sim \sqrt{\frac{2}{\pi n}} \frac{\cos\{n[\sqrt{y^2-1}-\arccos(1/y)]-\pi/4\}}{(y^2-1)^{1/4}}, \quad y > 1.$$
$$\tag{3.10}$$

The key point for our discussion is that the ratio $|J_n(ny_1)|/Y_n(ny)$ is exponentially small for large n and for fixed $0 < y < 1$. For $0 < y_1 < 1$, one has $J_n(ny_1)/Y_n(ny) \propto e^{-n[\zeta(y)+\zeta(y_1)]}$, and for $y_1 > 1$, we get $|J_n(ny_1)|/Y_n(ny) \propto e^{-n\zeta(y)}$.
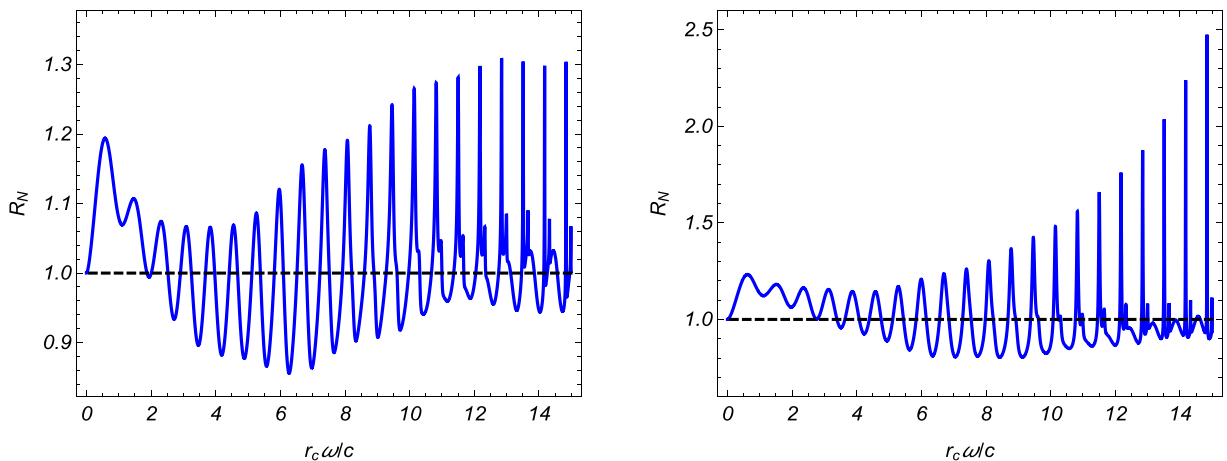

FIG. 3. The same as in Fig. 2, for $\varepsilon_0 = 3.8$, $\varepsilon_1 = 2.2$. For the left and right panels, $r_0/r_c = 1.2$ and $r_0/r_c = 1.1$.
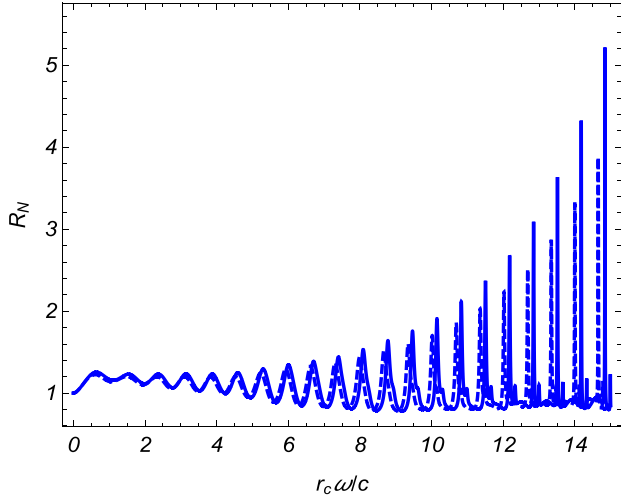
FIG. 4. The ratio R_N vs $\omega r_c/c$ for the electron energies $\mathcal{E}_e = 2$ MeV (full curve) and $\mathcal{E}_e = 10$ MeV (dashed curve). The graphs are plotted for $r_0/r_c = 1.05$, $\varepsilon_0 = 3.8$, $\varepsilon_1 = 2.2$.

With these asymptotic estimates, let us return to the expression (2.8) for the function α_n. As we have mentioned above, the roots of the equation $\alpha_n = 0$ determine the eigenmodes of the dielectric cylinder. Under the condition $\lambda_1^2 > 0$, this equation has no solutions. There are no eigenmodes in this range and all the radiated energy goes to infinity in the form of the CR with the spectral density (3.4). We can try to specify the conditions under which the function α_n would take its minimal value. In accordance with (3.4), that could correspond to large intensities for the CR. By taking into account that in accordance with the asymptotics given above, for large n and $\lambda_1 r_c < n$ the ratio $|J_n(\lambda_1 r_c)|/Y_n(\lambda_1 r_c)$ is exponentially small, we can expand α_n in terms of this ratio. In the next-to-leading order, we get

$$\alpha_n \approx \frac{\varepsilon_0}{\varepsilon_1 - \varepsilon_0} + \frac{1}{2}\sum_{l=\pm 1} g_{l,n} + \frac{i}{\pi \lambda_0 r_c}\sum_{l=\pm 1}\frac{l J_{n+l}(\lambda_0 r_c)g_{l,n}^2}{J_n(\lambda_0 r_c)Y_{n+l}^2(\lambda_1 r_c)},$$
(3.11)

where

$$g_{l,n} = \left[1 - \frac{\lambda_1}{\lambda_0}\frac{J_{n+l}(\lambda_0 r_c)Y_n(\lambda_1 r_c)}{J_n(\lambda_0 r_c)Y_{n+l}(\lambda_1 r_c)}\right]^{-1}.$$
(3.12)

Note that compared to the first two terms in the right-hand side of (3.11), the last term is of the order of $e^{-2n\zeta(\lambda_1 r_c/n)}$. From here, it follows that near the roots of the equation

$$\sum_{l=\pm 1} g_{l,n} + \frac{2\varepsilon_0}{\varepsilon_1 - \varepsilon_0} = 0,$$
(3.13)

the function α_n is exponentially small, $\alpha_n \propto e^{-2n\zeta(\lambda_1 r_c/n)}$. Of course, this does not yet mean that the radiation intensity at those points will be large because exponential factors may also come from the other functions in the last term of the right-hand side of (2.11).

We recall that under the condition $\lambda_1^2 > 0$, the equation $\alpha_n = 0$ has no solutions and there are no eigenmodes of the cylinder in that region. The mathematical reason is that the function is complex and the real and imaginary parts do not

become zero simultaneously. Unlike the function α_n, the function $g_{l,n}$ is real and the equation (3.13) may have solutions. In order to specify the conditions under which the roots exist, first we consider the case $\lambda_0^2 > 0$ when the Cherenkov condition for the material of the cylinder is obeyed. For $\lambda_0 r_c < n$, by using the asymptotics (3.8) and (3.10) for the functions $Y_n(\lambda_1 r_c)$ and $J_n(\lambda_0 r_c)$, to the leading order, Eq. (3.13) is reduced to $\sqrt{n^2 - \lambda_1^2 r_c^2}/\sqrt{n^2 - \lambda_0^2 r_c^2} = -\varepsilon_1/\varepsilon_0$. This shows that for large values of n and for $\lambda_1 r_c < n$, Eq. (3.13) has solutions under the condition $\lambda_0 r_c > n$. In particular, one should have $\varepsilon_0 > \varepsilon_1$. By making use of the uniform asymptotic expansion for the modified Bessel function $I_n(|\lambda_0|r_c)$, we can see that from (3.13), the same leading-order equation is obtained for $\lambda_0^2 < 0$. From that equation, as a necessary condition for the existence of the roots in the range $\lambda_0^2 < 0 < \lambda_1^2$, one gets $\varepsilon_0 < -\varepsilon_1$. In the leading order, the roots with respect to the angular frequency are given by

$$\omega \approx \frac{cn}{r_c}\left(\frac{\varepsilon_0 \varepsilon_1}{\varepsilon_0 + \varepsilon_1} - \frac{c^2}{v^2}\right)^{-1/2}.$$
(3.14)

Note that the inequality $\varepsilon_0 < -\varepsilon_1$ also appears as a necessary condition for the radiation of surface polaritons (see below). For the latter modes, one has $\lambda_1^2 < 0$ and they are localized near the cylinder boundary.

Having specified the necessary conditions for the appearance of the peaks, we can estimate the corresponding heights and widths. First of all, on the base of the asymptotics for the Neumann and Bessel functions in the expression (2.11) of the functions $f_n^{(p)}$, it can be seen that for the appearance of the peaks, an additional condition $\lambda_1 r_0 < n$ is required. Under this condition, for the Hankel function in (2.11), one has $H_n(\lambda_1 r_0) \approx iY_n(\lambda_1 r_0)$ and $f_n^{(p)} \propto e^{n\zeta(\lambda_1 r_0/n)}$. As a consequence, the heights of the peaks in the spectral distribution of the radiation intensity are estimated as $e^{2n\zeta(\lambda_1 r_0/n)}$. We have numerically checked that the locations of the peaks with respect to $\omega r_c/c$ in the graphs above are determined by the roots of Eq. (3.13) with high accuracy. For example, the peaks in Fig. 4 at $\omega r_c/c = 10.83, 11.51, 12.17, 12.85, 13.51, 14.18$ come from the terms in (3.4) with $n = 15, 16, 17, 18, 19, 20$, respectively. On the base of the asymptotic consideration given above, the widths of the peaks can be estimated as well. In order to do that, we expand the function α_n near the roots of Eq. (3.13). By using (3.11), it can be seen that the width of the peaks is determined by the last term in the right-hand side and is of the order of $\Delta\omega/\omega \propto e^{-2n\zeta(\lambda_1 r_c/n)}$. Note that in the estimates given above, we have assumed that the dielectric permittivity ε_0 is real. For complex permittivity $\varepsilon_0 = \varepsilon_0' + i\varepsilon_0''$, with real and imaginary parts ε_0' and ε_0'', the consideration that is presented is valid under the condition $e^{-2n\zeta(\lambda_1 r_c/n)} \gg |\varepsilon_0''/\varepsilon_0'|$. For $e^{-2n\zeta(\lambda_1 r_c/n)} < |\varepsilon_0''/\varepsilon_0'|$, the heights and the widths of the peaks are determined by the imaginary part of the permittivity.

Summarizing the discussion above, we conclude that though there are no eigenmodes of the waveguide in the range under consideration ($\lambda_1^2 > 0$), Eq. (3.13) may have roots and, for large values of n, they approximately obey the equation $\alpha_n = 0$ with exponential accuracy. In this sense, those roots can be termed "quasimodes" of the dielectric waveguide (for the discussion of quasibound waves on curved interfaces,

see, e.g., [19]). Unlike to the guided and surface modes (see below) which remain coupled to the waveguide during their propagation and exponentially decay in the exterior medium, the radiation on the quasimodes appears in the form of the CR giving rise to high narrow peaks in the spectral distribution of the radiation intensity under the conditions $\lambda_1 r_0 < n < \lambda_0 r_c$ for $\lambda_0^2 > 0$ and under the conditions $\lambda_1 r_0 < n$, $\varepsilon_0 < -\varepsilon_1$ for $\lambda_0^2 < 0$. In the latter case, for a given n, the angular frequencies of the peaks are given by (3.14). In the corresponding spectral range, one has a quasidiscrete part of the CR. The spectral peaks appear for large values of n and, hence, this effect is absent in the axially symmetric problems (coaxial motion of charges and beams), where only the mode $n = 0$ contributes to the radiation intensity. We expect that similar features of the radiation intensity may appear for other geometries of the interface (see, for example, Ref. [20] for the radiation on a dielectric ball).

In the consideration above, in order to have an exactly solvable problem, we have made a number of idealizations. The possibility of experimental observation of the features discussed requires further investigation by taking into account a number of additional factors that can affect the radiation characteristics. In particular, they include the finite thickness of the medium where the particle moves (the exterior medium in the problem under consideration), the finite length of the waveguide, the collective effects of the particles in the bunch when the bunch size is of the order of radiation wavelength or larger, and the shift of the particle trajectory from the one we have considered. Similar to the case of the standard Cherenkov radiation in dielectric plates, the finite thickness of the radiator will lead to broadening of the angular distribution of the radiation. We also expect broadening of the peaks in the spectral distribution.

The charge moving in a medium suffers multiple scattering and this restricts the mean length of a straight trajectory. The multiple scattering leads to beam broadening that is determined by root-mean-square (rms) scattering angle θ_{ms}. The influence of beam broadening on the Cherenkov radiation in a homogeneous medium has been investigated in the literature, both theoretically and experimentally (see, e.g., [21] and references therein). For small angles θ_{ms}, the beam broadening leads to an additional factor in the angular-frequency distribution of the radiated energy. Note that at relatively small energies, the multiple scattering may essentially restrict the length of the particle straight trajectory in a medium. For example, for an electron with energy 2 MeV, which we have taken above for illustrative purposes only, the lengths in quartz and teflon are of the order of 1 mm. With increasing energy, the scattering angle θ_{ms} decreases inversely proportional to the energy (see, for example, [22]) and the mean length of the straight trajectory increases. As already mentioned before, the features of the Cherenkov radiation that we have discussed are sensitive to the velocity of the particle and are not sensitive to the particle energy at relatively high energies. For example, for the values of the parameters corresponding to Fig. 4, the locations of the peaks and the corresponding heights are almost the same for all the energies larger than 10 MeV. Note that in general, the thickness of the exterior medium and the length of the waveguide can be different.

The charge moves in the exterior medium and the multiple scattering restricts the first parameter only.

An interesting possibility to escape multiple scattering was indicated in [2,23]. It has been argued that an empty channel along the particle trajectory in a solid dielectric does not affect the radiation intensity if the channel radius is smaller than the wavelength of the radiation. The Cherenkov radiation by an electron bunch moving in a hollow cylindrical channel in dielectric-lined waveguides has been experimentally observed in [10] for the electron energies $\mathcal{E}_e = 10$ MeV, 60 MeV and for the radii of the channel $r_c = 0.25$ mm, 0.1 mm, respectively. Hollow capillary tubes with dielectric walls are among the main elements in dielectric wakefield accelerators and in capillary-guided laser wakefield accelerators (see [24–26] and references therein). Such schemes provide relatively compact accelerating systems with large acceleration gradients. In related experiments the parameters of the electron bunch and the radius of the tube vary over wide ranges. For example, in [25], the experiments were performed for the beam energy 28.5 GeV, rms bunch radius 0.01 mm, rms bunch lengths from 0.01 to 0.1 mm, and tube inner diameter 0.1 mm. The corresponding parameters for the experiments described in [26] are given as 20.35 GeV, 0.03 mm, 0.025–0.05 mm, and 0.3 mm. In both cases, SiO_2 annular capillaries have been used. In [26], the length of the capillaries ranges from 1 to 15 cm. In our setup, a hollow cylinder along the particle trajectory, corresponding to the inner region of this kind of capillaries, will not influence the features of the Cherenkov radiation in the frequency range $\lesssim 1$ THz.

IV. ENERGY LOSSES

In addition to the radiation propagating at large distances from the cylinder, one can have radiation emitted by the charge on the eigenmodes of the cylindrical waveguide. The total energy losses per unit of path length can be evaluated in terms of the work done by the electromagnetic field on the charge,

$$\frac{dW}{dz} = q E_3 \big|_{r \to r_0, z \to vt, \phi \to \phi_0}. \tag{4.1}$$

Substituting the analog of the Fourier expansion (2.3) for the z component of the electric field, one gets

$$\frac{dW}{dz} = 4q \sum_{n=0}^{\infty} {}' \mathrm{Re}\left[\int_0^\infty dk_z \, E_{n3}(k_z, r_0) \right], \tag{4.2}$$

where the relation (2.14) is used for E_{n3}. By using the expression for the corresponding Fourier component (2.13), we obtain

$$\frac{dW}{dz} = q^2 \sum_{n=0}^{\infty} {}' \mathrm{Re}\left[\int_0^\infty dk_z \, \frac{k_z}{\varepsilon_1} \sqrt{\beta_1^2 - 1} \sum_{p=\pm 1} f_n^{(p)} H_n(\lambda_1 r) \right]. \tag{4.3}$$

Note that unlike the expression (3.4), the functions $f_n^{(p)}$ enter in the expression of the energy losses linearly.

By taking into account the formulas (2.13) and (2.11), the expression (4.2) is decomposed into two contributions:

$$\frac{dW}{dz} = \frac{dW^{(0)}}{dz} + \frac{dW^{(c)}}{dz}, \qquad (4.4)$$

where

$$\frac{dW^{(0)}}{dz}$$

$$= -2q^2 \lim_{r \to r_0} {\sum_{n=0}^{\infty}}' \mathrm{Re}\left[\int_0^{\infty} dk_z \frac{k_z}{\varepsilon_1}(\beta_1^2 - 1)J_n(\lambda_1 r_0)H_n(\lambda_1 r)\right]$$

$$(4.5)$$

corresponds to the losses in a homogeneous medium with permittivity ε_1, and

$$\frac{dW^{(c)}}{dz} = 2q^2 {\sum_{n=0}^{\infty}}' \mathrm{Re}\left\{ \int_0^{\infty} dk_z \frac{k_z}{\varepsilon_1}(\beta_1^2 - 1)\frac{H_n^2(\lambda_1 r_0)}{V_n^H} \right.$$

$$\left. \times \left[V_n^J + \frac{ik_z J_n(\lambda_0 r_c)}{\pi\sqrt{\beta_1^2 - 1}r_c\alpha_n} \sum_{p=\pm 1} p\frac{J_{n+p}(\lambda_0 r_c)}{V_{n+p}^H} \right] \right\}$$

$$(4.6)$$

is induced by the cylinder. This formula gives the expression for the losses in the general case of the dielectric permittivity for the cylinder.

First we consider the case when the Cherenkov condition for the exterior medium is satisfied, $\beta_1^2 > 1$. The part (4.5) is further simplified by using the formula

$${\sum_{n=0}^{\infty}}' J_n(\lambda_1 r_0)H_n(\lambda_1 r) = \frac{1}{2}H_0(\lambda_1(r - r_0)). \qquad (4.7)$$

The real part of the latter is $J_0(\lambda_1(r - r_0))/2$ and, taking the limit $r \to r_0$ in (4.5), we get

$$\frac{dW^{(0)}}{dz} = -\frac{q^2}{c^2}\int_{\beta_1 > 1} d\omega\,\omega\big(1 - 1/\beta_1^2\big), \qquad (4.8)$$

which gives the standard expression for the Cherenkov radiation in a homogeneous medium. Under the condition $\beta_1^2 > 1$, one has $\lambda_1^2 > 0$ and it can be shown that the equation $\alpha_n = 0$ has no solutions with respect to k_z and the integrand in (4.6) is regular on the positive semiaxis of k_z. For real values of $\varepsilon_0 = \varepsilon_0(\omega)$, the energy losses are in the form of the radiation (here and below, we will not consider the ionization losses that correspond to the zeros of the function ε_1). For the spectral density of the energy radiated per unit time, we find

$$\frac{dI}{d\omega} = -v\frac{d^2W}{dz\,d\omega} = \frac{q^2 v}{c^2}\,\omega\left(1 - \frac{1}{\beta_1^2}\right)\left(1 - 2{\sum_{n=0}^{\infty}}' \mathrm{Re}\left\{\frac{H_n^2(\lambda_1 r_0)}{V_n^H}\right.\right.$$

$$\left.\left. \times \left[V_n^J + \frac{ik_z J_n(\lambda_0 r_c)}{\pi\sqrt{\beta_1^2 - 1}r_c\alpha_n} \sum_{p=\pm 1} p\frac{J_{n+p}(\lambda_0 r_c)}{V_{n+p}^H} \right] \right\}\right).$$

$$(4.9)$$

For $\beta_1^2 > 1$, there is no radiation on the eigenmodes of the cylinder and (4.9) corresponds to the CR in the exterior

medium. We have numerically checked that the formula (4.9) gives the same results as (3.4) for both the cases $\lambda_0^2 > 0$ and $\lambda_0^2 < 0$. Note that in (4.9), the contribution corresponding to the radiation in a homogeneous medium (the part with the first term in figure braces) is explicitly separated.

V. RADIATION ON GUIDED MODES OF THE WAVEGUIDE

Now we consider the case when the Cherenkov condition for the exterior medium is not obeyed, $\beta_1 < 1$. In this case, one has $\lambda_1 = i|\lambda_1|$ and the expression in the square brackets of (4.5) is purely imaginary. As a consequence, we get $dW^{(0)}/dz = 0$ and the radiation in a transparent homogeneous medium is absent. Introducing the modified Bessel functions $I_n(x)$ and $K_n(x)$, the expression for the energy losses is presented as

$$\frac{dW}{dz} = -\frac{2q^2}{\pi}{\sum_{n=0}^{\infty}}' \mathrm{Im}\left\{ \int_0^{\infty} dk_z \frac{k_z}{\varepsilon_1}\big(1 - \beta_1^2\big)\frac{K_n^2(|\lambda_1|r_0)}{V_n^{J,K}} \right.$$

$$\left. \times \left[2V_n^{J,I} - \frac{k_z J_n(\lambda_0 r_c)}{r_c\sqrt{1 - \beta_1^2}\alpha_n} \sum_{p=\pm 1} \frac{J_{n+p}(\lambda_0 r_c)}{V_{n+p}^{J,K}} \right] \right\},$$

$$(5.1)$$

with $(F = I, K)$

$$V_n^{J,F} = J_n(\lambda_0 r_c)\partial_{r_c}F_n(|\lambda_1|r_c) - F_n(|\lambda_1|r_c)\partial_{r_c}J_n(\lambda_0 r_c) \quad (5.2)$$

and

$$\alpha_n = \frac{\varepsilon_0}{\varepsilon_1 - \varepsilon_0} + \frac{1}{2}\sum_{l=\pm 1}\left[1 + l\frac{|\lambda_1|}{\lambda_0}\frac{J_{n+l}(\lambda_0 r_c)K_n(|\lambda_1|r_c)}{J_n(\lambda_0 r_c)K_{n+l}(|\lambda_1|r_c)}\right]^{-1}.$$

$$(5.3)$$

For real values of ε_0, the integrand in (5.1) is real on the real axis of k_z and the nonzero contributions to the integral may come from the possible poles on the real axis only. We can see that the integral is regular at the zeros of the functions $V_{n\pm 1}^{J,K}$ and $V_n^{J,K}$. Hence, the only nonzero contributions come from the zeros of the function α_n. These zeros with respect to k_z we will denote by $k_z = k_{n,s} > 0$, where $s = 1, 2, \ldots$ enumerates the roots for a given n, $k_{n,s+1} > k_{n,s}$. These roots determine the eigenmodes of the dielectric cylinder (the equation $\alpha_n = 0$ is easily transformed to the form given, for example, in [27]). For $n = 0$, the equation for those modes is simplified to

$$\varepsilon_0\frac{\sqrt{1 - \beta_1^2}}{\sqrt{\beta_0^2 - 1}}\frac{J_1(\lambda_0 r_c)}{J_0(\lambda_0 r_c)} + \varepsilon_1\frac{K_1(|\lambda_1|r_c)}{K_0(|\lambda_1|r_c)} = 0. \qquad (5.4)$$

Note that the product $k_z r_c = k_{n,s} r_c$ does not depend on r_c and is a function of two parameters, $\varepsilon_0/\varepsilon_1$ and β_1,

$$k_{n,s} r_c = f(\varepsilon_0/\varepsilon_1, \beta_1). \qquad (5.5)$$

In order to evaluate the integral in (5.1), one needs to specify the integration contour near the poles $k_z = k_{n,s}$. In this section, we will consider the spectral range where $\lambda_0^2 > 0$. The corresponding eigenmodes $k_{n,s}$ are the guided modes of the dielectric cylinder. For those modes, the radial dependence of the Fourier components for the fields inside the cylinder is

expressed in terms of the Bessel function $J_n(\lambda_0 r)$. In order to specify the contour, we note that in physically realistic problems, the permittivity ε_0 has an imaginary part, $\varepsilon_0 = \varepsilon_0' + i\varepsilon_0''$. We consider α_n from (5.3) as a function of k_z and ε_0, $\alpha_n = \alpha_n(k_z, \varepsilon_0)$. Note that in the presence of dispersion, one has $\varepsilon_0 = \varepsilon_0(\omega) = \varepsilon_0(k_z v)$ and the second argument is a function of k_z as well. Assuming that $|\varepsilon_0''/\varepsilon_0'| \ll 1$, the dominant contribution to the integral in (5.1) comes from the region near $k_z = k_{n,s}$, where $k_{n,s}$ is the sth root of the equation $\alpha_n(k_z, \varepsilon_0') = 0$. First we write $\alpha_n(k_z, \varepsilon_0) \approx \alpha_n(k_z, \varepsilon_0') + i\varepsilon_0'' \partial_{\varepsilon_0'} \alpha_n(k_z, \varepsilon_0')$ and then expand near $k_z = k_{n,s}$:

$$\alpha_n(k_z, \varepsilon_0) \approx \partial_{k_z}\alpha_n(k_z, \varepsilon_0')|_{k_z=k_{n,s}}(k_z - k_{m,s} + i\varepsilon_0'' b_{n,s}), \quad (5.6)$$

where

$$b_{n,s} = \frac{\partial_{\varepsilon_0}\alpha_n(k_z, \varepsilon_0)}{\partial_{k_z}\alpha_n(k_z, \varepsilon_0)}\bigg|_{k_z=k_{n,s}, \varepsilon_0=\varepsilon_0'}. \quad (5.7)$$

Note that though ε_0 may depend on k_z, the derivative $\partial_{\varepsilon_0}\alpha_n(k_z, \varepsilon_0)$ is taken for the fixed value of k_z. As for the denominator, $\partial_{k_z}\alpha_n(k_z, \varepsilon_0) = (d/dk_z)\alpha_n(k_z, \varepsilon_0)$, in the presence of dispersion $\varepsilon_0 = \varepsilon_0(k_z v)$, the derivative is taken with respect to both of the arguments. From (5.6), we see that the pole of the integrand in (5.1) is located at $k_z = k_{m,s} - i\varepsilon_0'' b_{n,s}$. We have numerically checked that the numerator in (5.7) is negative for $\lambda_0^2 > 0$ and the sign of $b_{n,s}$ is determined by the sign of the denominator. The latter will be denoted as $\sigma_{n,s} = \text{sgn}[\partial_{k_z}\alpha_n(k_z, \varepsilon_0')]|_{k=k_{n,s}} = -\text{sgn}(b_{n,s})$. By taking into account that $\varepsilon_0''(\omega) > 0$ for $\omega > 0$, from here we conclude that for $\lambda_0^2 > 0$ in (5.1), the poles $k_z = k_{n,s}$ should be avoided from above for $\sigma_{n,s} < 0$ and from below for $\sigma_{n,s} > 0$ by small semicircles in the complex plane k_z. The integrals over these semicircles are expressed in terms of the corresponding residues. Returning to the case of real ε_0, $\varepsilon_0 = \varepsilon_0'$, for the energy radiated per unit time we get

$$I = \sum_{n=0}^{\infty}{}' \sum_s I_{n,s} = -v\frac{dW}{dz}, \quad (5.8)$$

where the radiation intensity on the angular frequency $\omega_{n,s} = vk_{n,s}$ is given by

$$I_{n,s} = -2\delta_n q^2 \frac{v}{\varepsilon_1}\sqrt{1-\beta_1^2}k_z^2 \frac{K_n^2(|\lambda_1|r_0)}{V_n^{J,K}} \frac{J_n(\lambda_0 r_c)}{r_c|\alpha_n'(k_z)|}$$
$$\times \sum_{p=\pm 1} \frac{J_{n+p}(\lambda_0 r_c)}{V_{n+p}^{J,K}}\bigg|_{k_z=k_{n,s}}. \quad (5.9)$$

Here, $\alpha_n'(k_z) = \partial_{k_z}\alpha_n(k_z, \varepsilon_0)$, $\delta_0 = 1/2$, and $\delta_n = 1$ for $n = 1, 2, \ldots$. This expression determines the radiation intensity on the guided modes of the dielectric waveguide. If the Cherenkov condition for the surrounding medium is not satisfied, the CR emitted inside the cylinder is totally reflected from the separating boundary.

The dependence of the radiation intensity on the distance of the charge from the waveguide axis enters through the function $K_n^2(|\lambda_1|r_0)$. For large values of r_0, the intensity is exponentially small. For large values of $|\lambda_1|r_c \gg 1$, the intensity is suppressed by the factor $e^{-2|\lambda_1|(r_0-r_c)}$. Hence, the guided modes of the waveguide are mainly radiated on the

TABLE I. The first eigenvalues for $k_z r_c$ for different values of the azimuthal number n.

n	0	1	2	3	4	5	10	15	20
$k_{n,1}r_c$	1.689	0.886	1.971	2.866	3.685	4.465	8.124	11.613	15.027

frequencies

$$\omega_{n,s} \lesssim \frac{v}{\sqrt{1-\beta_1^2}(r_0-r_c)}. \quad (5.10)$$

For $n \geqslant 1$, one has $k_{n+1,1} > k_{n,1}$. In Table I, we present $k_{n,1}r_c$ for $\mathcal{E}_e = 2$ MeV, $\varepsilon_0 = 3.8$, $\varepsilon_1 = 1$, and for several values of n. As seen, for $n \geqslant 1$, the first root $k_{n,1}r_c$ is of the order of n.

Assuming that $|\lambda_j|r_c \gg n$, the asymptotic expression for the roots $k_{n,s}$ is found by using the asymptotic formulas for the cylinder functions for large arguments,

$$k_{n,2l+1}r_c \approx \frac{1}{\sqrt{\beta_0^2-1}}\left[\frac{n\pi}{2} + \frac{\pi}{4} - \arctan\left(\frac{\varepsilon_1}{\varepsilon_0}\sqrt{\frac{\beta_0^2-1}{1-\beta_1^2}}\right) + \pi l\right], \quad (5.11)$$

where $l \gg 1$ and $k_{n,2l} < k_{n,2l+1}$ is close to (5.11). For a given n, the frequency $\omega_{n,s}$ of the guided mode increases with increasing s and the upper limit of the summation over s in (5.8) is determined from the Cherenkov condition, $v\varepsilon_0(\omega_{n,s})/c > 1$.

In the figures below, we plot the number of quanta radiated on a given mode $k_{n,s}$ per unit length of the charge trajectory,

$$N_{n,s} = \frac{I_{n,s}}{\hbar\omega_{n,s}v}. \quad (5.12)$$

Figure 5 presents the number of the radiated quanta as a function of $\omega_{n,s}r_c/c$ for given n and for different values of s. For the parameters, we have taken $\mathcal{E}_e = 2$ MeV, $\varepsilon_0 = 3.8$, $\varepsilon_1 = 1$, and $r_0/r_c = 1.05$. The left and right panels correspond to $n = 1$ and $n = 2$, respectively. As seen, for fixed n and starting from $s = 2$, the roots $k_{n,s}$ come in pairs which are close to each other. The radiation intensity on the first root in the pair is much smaller than on the second one. For example, $N_{1,2}/N_{1,3} \approx 0.0026$ and $N_{2,2}/N_{2,3} \approx 0.001$. The radiation on the modes with $n = 0$ is essentially smaller compared to the cases presented in Fig. 5. For the same values of the parameters, one has $\omega_{0,1}r_c/c \approx 1.63$ and $r_c N_{0,1} \approx 0.026q^2/(\hbar c)$. The corresponding results for $n = 5$ (circles), $n = 10$ (diamonds), and $n = 20$ (squares) are presented in Fig. 6.

Note that the numerical results above are given in relative units and can be used to estimate the radiation intensity in a wide range of frequencies. The absolute values for the radiation frequencies depend on the diameter of the cylindrical waveguide and are restricted by the condition (5.10). For available waveguides, the diameter may vary over a wide range starting from 50 nm (used for optical wave guiding). In particular, various types of terahertz waveguides, with radius of the order of 1 mm, have been discussed in the literature. Note that in the figures given above (and also given below for the radiation of surface polaritons), we have plotted the
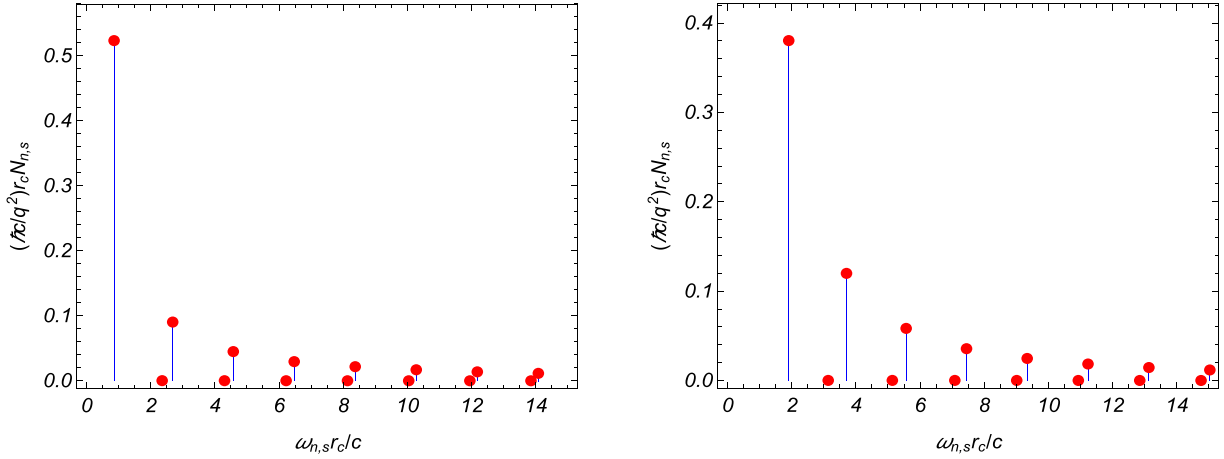
FIG. 5. The number of quanta radiated on guided modes of the cylinder vs $\omega_{n,s}r_c/c$ for $n=1$ (left panel) and $n=2$ (right panel). The data are presented for $\mathcal{E}_e = 2$ MeV, $\varepsilon_0 = 3.8$, $\varepsilon_1 = 1$, and $r_0/r_c = 1.05$.

number of quanta radiated from the part of the particle trajectory equal to the cylinder radius. For waveguides with small radii, the number of quanta radiated from the unit length of the trajectory can be fairly large. However, in the experimental conditions, a number of additional factors must be taken into account. In particular, the lower limit of the distance from the cylinder surface $r_0 - r_c$, appearing in the condition (5.10) is restricted by the bunch radius. It is of interest to note that for a bunch moving in vacuum ($\varepsilon_1 = 1$), the upper limit in (5.10) linearly increases with increasing beam energy. For example, considering the parameters of the bunch used in the experiments of Ref. [10] (bunch energy 60 MeV and radius 0.1 mm) and taking $r_0 - r_c = 1$ mm, for the upper limit of the frequency $\omega/(2\pi)$, obtained from the right-hand side of (5.10), we get ≈ 5.6 THz.

VI. EMISSION OF SURFACE POLARITONS

In this section, we consider the radiation on the modes of the dielectric cylinder with $\lambda_j^2 < 0$, $j = 0, 1$, that correspond to surface polaritons. For the Fourier components of the fields with a given n, the radial dependence is described
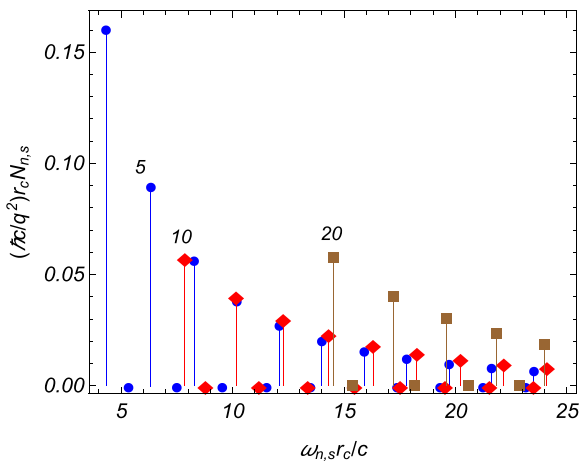

FIG. 6. The same as in Fig. 5, for $n = 5, 10, 20$.

by the function $K_n(|\lambda_1|r)$ in the region $r > r_c$ and by the function $I_n(|\lambda_0|r)$ inside the cylinder, $r < r_c$, and these modes correspond to surface waves. Depending on the electromagnetic properties of the contacting media, various types of surface waves can be excited on the separating boundary. Among them, motivated by wide applications in light-emitting devices, surface imaging, data storage, surface-enhanced Raman spectroscopy, biomedicine, plasmonic solar cells, etc., the surface plasmon polaritons have attracted a great deal of attention [28]. They are evanescent electromagnetic waves propagating along a metal-dielectric interface as a result of collective oscillations of electrons coupled to an electromagnetic field. Among the most important properties of surface plasmon polaritons is the possibility for concentration of the fields beyond the diffraction limit that enhances the local field strengths by several orders of magnitude. Other types of active media instead of metals can also support surface polariton modes. Examples are organic and inorganic dielectrics, ionic crystals, doped semiconductors, and metamaterials [29]. An important advantage of these materials is the possibility to control the parameters in the dispersion relations for dielectric permittivity and magnetic permeability. In particular, they can be used for the extension of plasmonics to the infrared and terahertz frequency ranges.

In the problem under consideration, the formula for the energy losses in the form of surface polaritons is obtained from (5.1) introducing, instead of the functions $J_n(\lambda_0 r_c)$ and $J_{n\pm1}(\lambda_0 r_c)$, the modified Bessel functions $I_n(|\lambda_0|r_c)$ and $I_{n\pm1}(|\lambda_0|r_c)$. Similar to the case of guided modes, we can see that for real k_z, the integrand is real and, hence, the only nonzero contribution to the integral comes from the poles of the integrand. As before, the latter correspond to the zeros of the function α_n. In the case under consideration, this function is written as

$$\alpha_n = \frac{\varepsilon_0}{\varepsilon_1 - \varepsilon_0} + \frac{1}{2} \sum_{l=\pm1} \left[1 + \frac{|\lambda_1|}{|\lambda_0|} \frac{I_{n+l}(|\lambda_0|r_c)K_n(|\lambda_1|r_c)}{I_n(|\lambda_0|r_c)K_{n+l}(|\lambda_1|r_c)} \right]^{-1}.$$

(6.1)

The equation $\alpha_n = 0$ determines the dispersion relation for the surface modes (see, for example, [31]). By taking into
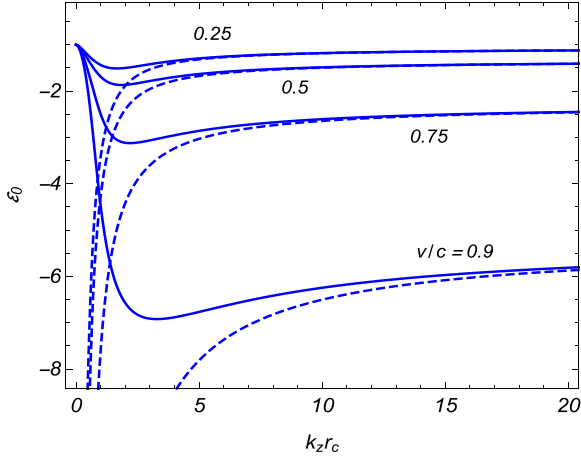
FIG. 7. The localization of the eigenmodes of the cylinder with respect to $k_z r_c$ for $n = 0$ (dashed curves) and $n = 1$ (full curves). For the surrounding medium, we have taken $\varepsilon_1 = 1$ and the numbers near the curves are the values of v/c.

account that the term with the ratios of the modified Bessel functions is always positive, we conclude that the equation may have solutions if and only if $0 < 1/(1 - \varepsilon_1/\varepsilon_0) < 1$ or, equivalently, under the condition $\varepsilon_1/\varepsilon_0 < 0$. Hence, in order to have eigenmodes of the cylinder with $\lambda_0^2 < 0$, the dielectric permittivities of the cylinder and of the surrounding medium should have opposite signs. Of course, this is a result that is well known for planar interfaces as well.

As before, we will denote by $k_{n,s}$ the eigenvalues for k_z, being the roots of the equation $\alpha_n = 0$. Unlike the case of guided modes, because of monotonicity of the modified Bessel functions, the equation $\alpha_n = 0$ for surface polaritons has a finite number of solutions. For a given n, we can have one or two roots. This feature is illustrated in Fig. 7 where the roots with respect to $k_z r_c$ are plotted versus ε_0 for $\varepsilon_1 = 1$ and for several values of the ratio v/c (numbers near the curves). The dashed and full curves correspond to $n = 0$ and $n = 1$, respectively. By taking into account that the product $k_{n,s} r_c$ depends on the parameters through the combinations $\varepsilon_0/\varepsilon_1$ and β_1, we see that Fig. 7 describes the distribution of the roots for $\varepsilon_1 \neq 1$ as well. In the limit $k_z r_c \to \infty$, the curves tend to the limiting value $\varepsilon_0 = \varepsilon_0^{(\infty)}$, which depends on the ratio v/c and does not depend on n. Below it will be shown that

$$\varepsilon_0^{(\infty)} = -\frac{\varepsilon_1}{1 - \beta_1^2}. \quad (6.2)$$

As seen from the graphs, for $n = 0$, one has a single root in the region $\varepsilon_0 < \varepsilon_0^{(\infty)}$ and there are no surface modes in the range $\varepsilon_0 > \varepsilon_0^{(\infty)}$. For $n \geqslant 1$, the surface modes are present in the region $\varepsilon_0^{(m)} \leqslant \varepsilon_0 < -\varepsilon_1$ (see the asymptotic analysis below), where the minimal value $\varepsilon_0^{(m)}$ depends on n and v/c. For ε_0 close to the minimal value, one has two roots, whereas in the remaining range a single root exists. In the limit $v/c \to 0$, one has $\varepsilon_0^{(m)} \to -\varepsilon_1$ and for $v/c \ll 1$ the surface modes are present in the narrow range for the permittivity ε_0 with the length of the order of β_1^2.

The distribution of the roots presented in Fig. 7 can be understood qualitatively considering the asymptotic behavior

of the function α_n from (6.1). For $k_z r_c \gg n + 1$, assuming also that $|\lambda_j| r_c \gg n + 1$, we get

$$\alpha_n \approx \frac{\varepsilon_0}{\varepsilon_1 - \varepsilon_0} + \left(1 + \sqrt{\frac{1 - \beta_1^2}{1 - \beta_0^2}}\right)^{-1}\left(1 + \frac{1}{2|\lambda_0| r_c}\right). \quad (6.3)$$

From here it follows that for the graphs in Fig. 7, one has $\varepsilon_0 \to \varepsilon_0^{(\infty)} \equiv -\varepsilon_1/(1 - \beta_1^2)$ in the limit $k_z r_c \to \infty$. Note that this asymptotic does not depend on n. In the opposite limit of small $k_z r_c \ll 1$, we get

$$\alpha_0 \approx \frac{\varepsilon_1}{\varepsilon_1 - \varepsilon_0} + \frac{1}{4}(1 - \beta_1^2)(k_z r_c)^2 \ln(k_z r_c),$$

$$\alpha_1 \approx \frac{1}{2}\frac{\varepsilon_1 + \varepsilon_0}{\varepsilon_1 - \varepsilon_0} - \frac{1}{4}(1 - \beta_0^2)(k_z r_c)^2 \ln(k_z r_c), \quad (6.4)$$

and

$$\alpha_n \approx \frac{1}{2}\frac{\varepsilon_1 + \varepsilon_0}{\varepsilon_1 - \varepsilon_0} + k_z^2 r_c^2 \frac{2 + [(n-1)\varepsilon_1 - (n+1)\varepsilon_0]v^2/c^2}{8n(n^2 - 1)}, \quad (6.5)$$

for $n > 1$. From these asymptotic expressions, it follows that for the roots of the equation $\alpha_0 = 0$, we have $\varepsilon_0 \to -\infty$ in the limit $k_z r_c \to 0$. This feature is seen in Fig. 7 (dashed curves). For $n \geqslant 1$, the asymptotic expressions (6.4) and (6.5) imply that for the roots of $\alpha_n = 0$, one has $\varepsilon_0 \to -\varepsilon_1$ in the limit $k_z r_c \to 0$. Again, this is confirmed by Fig. 7 (full curves).

In considerations of surface polaritons the allowance for the dispersion of the dielectric permittivity of the cylinder, $\varepsilon_0 = \varepsilon_0(\omega)$, is required. Among the most popular models used in surface plasmonics (see, for example, [28,29]) is the Drude-type dispersion,

$$\varepsilon_0(\omega) = \varepsilon_\infty - \frac{\omega_p^2}{\omega^2 + i\gamma\omega}, \quad (6.6)$$

where ε_∞ is the background dielectric constant, ω_p is the plasma frequency, and γ is the characteristic collision frequency or the damping coefficient. The plasma frequency can be tuned by changing the carrier concentrations in the material. For example, in the terahertz range, doped semiconductors are used. Alternatively, one can control the electromagnetic properties by using artificially constructed materials.

In the discussion below, we will ignore the imaginary part in (6.6), assuming that the absorption is small. In the corresponding model, the surface polaritons are radiated in the spectral range $\omega < \omega_p/\sqrt{\varepsilon_\infty}$. Let us consider the properties of those modes in the asymptotic regions of the dimensionless parameter $\omega_p r_c/v$. For $\omega_p r_c/v \ll 1$, one has $|\lambda_j| r_c \ll 1$ and, for α_0, we have the asymptotic expression (6.4). As already mentioned, from that asymptotic, it follows that $-\varepsilon_0 \gg 1$ or $\omega/\omega_p \ll 1$ for the $n = 0$ modes (for composite materials with high negative permittivity, see, for example, [30] and references therein). For the dispersion (6.6) with $\gamma = 0$, from the asymptotic expression of α_0 for the frequencies of $n = 0$ surface polaritons in the range $\omega_p r_c/v \ll 1$, one gets

$$\frac{\omega}{\omega_p} \approx \frac{(\omega_p r_c/v)^{-1}}{\sqrt{1 - \beta_1^2}} \exp\left[-\frac{2\varepsilon_1(\omega_p r_c/v)^{-2}}{1 - \beta_1^2}\right]. \quad (6.7)$$
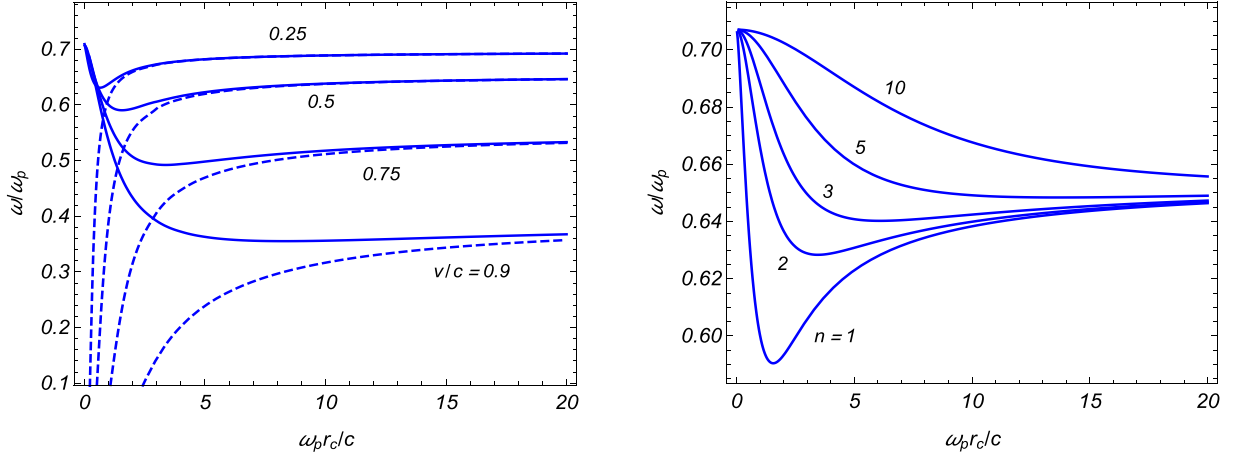
FIG. 8. Eigenfrequencies of the cylinder corresponding to surface polaritons vs $\omega_p r_c/c$ for the dispersion law (6.6) with $\gamma = 0$ and for $\varepsilon_1 = 1$. On the left panel, the full and dashed curves correspond to the modes with $n = 1$ and $n = 0$, respectively, and the numbers near the curves are the values of the ratio v/c. The graphs on the right panel are plotted for $v/c = 0.5$ and the numbers near the curves correspond to the values of n.

For the modes with $n \geqslant 1$ and under the condition $\omega_p r_c/v \ll 1$, we use the asymptotics (6.4) and (6.5). From those expressions, in combination with (6.6), it follows that one should have $|\varepsilon_0 + \varepsilon_1| \ll 1$. By taking into account (6.6), for the surface polariton modes with $n \geqslant 1$, we obtain

$$\frac{\omega}{\omega_p} \to \frac{1}{\sqrt{\varepsilon_\infty + \varepsilon_1}}, \quad \omega_p r_c/v \to 0. \quad (6.8)$$

In the opposite limit $\omega_p r_c/v \gg n + 1$, one has $|\lambda_j| r_c \gg n + 1$ and we can use the asymptotic expression (6.3). From the equation $\alpha_n = 0$, in combination with $\varepsilon_0/\varepsilon_1 < 0$, it follows that $\varepsilon_0/\varepsilon_1 \approx -1/(1 - \beta_1^2)$. For the dispersion (6.6), this gives

$$\frac{\omega^2}{\omega_p^2} \approx \frac{1}{\varepsilon_\infty + \varepsilon_1/(1 - \beta_1^2)}, \quad (6.9)$$

in the asymptotic region $\omega_p r_c/v \gg n + 1$.

In the left panel of Fig. 8, for dispersion law (6.6) with $\varepsilon_\infty = 1$ and $\gamma = 0$, we present the frequencies for the eigenmodes of the cylinder as functions of the plasma frequency. The full and dashed curves correspond to $n = 1$ and $n = 0$, respectively. The numbers near the curves are the values of the ratio v/c. The right panel of Fig. 8 presents the frequencies of the eigenmodes for different values of n (numbers near the curves). From the data plotted in Fig. 8, we see that for $n = 0$, the frequencies of the surface polaritons are in the range

$$\omega < \omega_p \left(\varepsilon_\infty + \frac{\varepsilon_1}{1 - \beta_1^2} \right)^{-1/2}. \quad (6.10)$$

For the frequencies of the modes with $n \geqslant 1$, in addition to the upper limit in (6.10), one has a lower limit: $\omega \geqslant \omega^{(m)}$. The limiting frequency increases with increasing n and tends to $\omega_p/\sqrt{\varepsilon_\infty + \varepsilon_1/(1 - \beta_1^2)}$ for large values of n.

Having clarified the distribution of the eigenmodes, we turn to the radiation intensity for surface polaritons. Similar to the case of guided modes, in order to specify the integration contour near the poles of the integrand in (5.1), we introduce an imaginary part of the permittivity ε_0 and use the expansion (5.6). The poles are located at $k_z = k_{n,s} - i\varepsilon_0'' b_{n,s}$, where $b_{n,s}$ is

defined by (5.7). We have checked numerically that for $\lambda_0^2 < 0$, one has $\partial_{\varepsilon_0'} \alpha_n(k_{n,s}, \varepsilon_0') > 0$. From here, it follows that the poles $k_z = k_{n,s}$ should be avoided from above for $\sigma_{n,s} > 0$ and from below for $\sigma_{n,s} < 0$ by small semicircles in the complex plane k_z. The energy radiated per unit time is presented as (5.8), where the radiation intensity for surface polaritons of the angular frequency $\omega_{n,s} = v k_{n,s}$ is expressed as

$$I_{n,s} = 2\delta_n q^2 \frac{v}{\varepsilon_1} \sqrt{1 - \beta_1^2} k_z^2 \frac{K_n^2(|\lambda_1| r_0)}{V_n^K} \frac{I_n(|\lambda_0| r_c)}{r_c |\alpha_n'(k_z)|}$$

$$\times \sum_{p=\pm 1} \frac{I_{n+p}(|\lambda_0| r_c)}{V_{n+p}^K} \Bigg|_{k_z = k_{n,s}}, \quad (6.11)$$

where $|\lambda_j| = k_z \sqrt{1 - \beta_j^2}$,

$$V_n^F = I_n(|\lambda_0| r_c) \partial_{r_c} F_n(|\lambda_1| r_c) - F_n(|\lambda_1| r_c) \partial_{r_c} I_n(|\lambda_0| r_c), \quad (6.12)$$

for $F = I, K$. Note that one has $V_n^K < 0$. Similar to the case of the guided modes, the radiation intensity is suppressed by the factor $e^{-2|\lambda_1|(r_0 - r_c)}$ for the modes with $|\lambda_1| r_c \gg 1$. Unlike the guided modes, there is no velocity threshold for the generation of surface polaritons.

Let us consider asymptotic estimates of the radiation intensity for the dispersion relation (6.6) with $\gamma = 0$. In accordance with the analysis given above, in the limit $v \to 0$, one has $\omega \to \omega_p/\sqrt{\varepsilon_1 + \varepsilon_\infty}$. By taking into account that $|\lambda_j| r_c \approx \omega r_c/v$, we see that the arguments of the modified Bessel functions in (6.11) are large. By using the corresponding asymptotic expressions, we conclude that in the limit $v \to 0$, the radiation intensity is suppressed by the factor $\exp[-2\omega_p(r_0 - r_c)/(v\sqrt{\varepsilon_1 + \varepsilon_\infty})]$. Now we turn to the behavior of the radiation intensity in the limiting regions of the combination $\omega_p r_c/v$. In the region $\omega_p r_c/v \ll 1$ and for the modes $n = 0$, we get $I_{0,s} \propto (\omega/\omega_p)^2/(\omega_p r_c/v)^2$, where the ratio ω/ω_p is given by (6.7). The corresponding radiation intensity is exponentially small. For the surface modes with $n \geqslant 1$, the radiation intensity in the same region is estimated
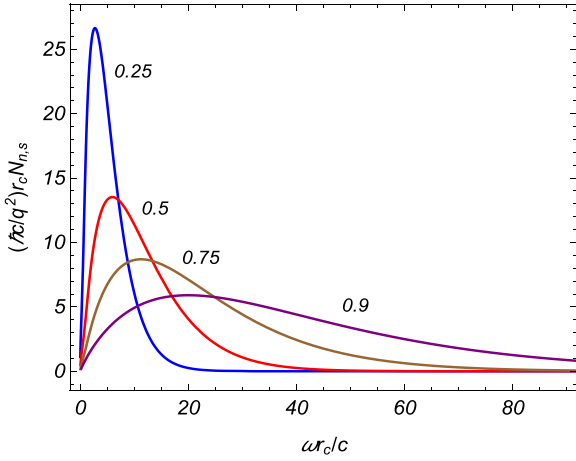
FIG. 9. The spectral distribution of the number of radiated surface polaritons on the modes with $n = 0$ for a cylinder immersed in the vacuum. The numbers near the curves are the values for v/c.

as

$$I_{n,s} \approx \frac{2q^2 v}{r_c^2} \frac{(r_c/r_0)^{2n}(\omega_p r_c/v)^2}{n(\varepsilon_\infty + \varepsilon_1)^2}. \qquad (6.13)$$

The corresponding frequencies are given by (6.9) and the radiation intensity is suppressed by the factor $(\omega_p r_c/v)^2$. In the opposite limit, $\omega_p r_c/v \gg n + 1$, the radiation intensity is estimated as

$$I_{n,s} \approx \frac{2q^2 \omega_p}{r_0} \frac{(\omega/\omega_p)^3}{1 - \beta_1^2/2} \exp\left[-2(r_0 - r_c)\frac{\omega}{v}\sqrt{1 - \beta_1^2}\right], \qquad (6.14)$$

with the radiation frequency from (6.9). Similar to the case of the guided modes, the frequency of the radiated surface polaritons is restricted by the condition (5.10). For the values of the bunch parameters discussed at the end of the previous section, the upper limit of the frequency for surface polaritons is of the order of 10 THz. On the other hand, our consideration is restricted by the condition $\omega \gg \gamma$ that is required to neglect the imaginary part of the dielectric permittivity in (6.6). For

metals, the ratio $\gamma/(2\pi)$ is of the order of 10 THz and the approximation used in deriving (6.11) is not valid for the above-mentioned values of the bunch characteristics. Note that the formula (4.3) for the energy losses is valid for the general case of the complex function $\varepsilon_0(\omega)$. In the presence of the imaginary part of $\varepsilon_0(\omega)$, in addition to the radiation part, dW/dz also contains other types of energy losses.

In Fig. 9, we have displayed the number of the radiated quanta for surface polaritons as a function of the frequency for the modes with $n = 0$ and for $\varepsilon_1 = 1$, $r_0/r_c = 1.05$. The numbers near the curves are the values of the ratio v/c. Note that different frequencies correspond to different values of the permittivity ε_0. The value for ε_0 corresponding to a given frequency can be found from the data depicted in Fig. 7. We see that the number of the radiated quanta is large enough compared to the case of the radiation of guided modes.

Here, a comment is in order. In the numerical evaluations corresponding to Fig. 9, for a given value of ε_0, with fixed ε_1 and v, we solve the equation $\alpha_n = 0$ with respect to $k_z r_c$. At this step, for a given ε_0, the specific form of the dispersion is not required. The latter is needed in the numerical evaluation of the radiation intensity. Indeed, the radiation intensity contains the derivative $\alpha'_n(k_z)$. By taking into account the relation $\omega = k_z v$, in the expression for $\alpha'_n(k_z)$ the derivative $\partial_\omega \varepsilon_0(\omega)$ will enter coming from the terms in (6.1) with λ_0 and from the first term in the right-hand side. Hence, for the evaluation of the radiation intensity on a given frequency ω, in addition to $\varepsilon_0(\omega)$, the value of the derivative $\partial_\omega \varepsilon_0(\omega)$ is required. Plotting the graphs in Fig. 9, we have assumed that the dispersion is weak and the part of the derivative $\alpha'_n(k_z)$ containing $\partial_\omega \varepsilon_0(\omega)$ has been ignored. In the spectral range with $\varepsilon_0 < 0$, this idealization may lead to problems. For example, a problem appears in the evaluation of the radiation intensity on the mode $n = 1$. In the absence of dispersion, there exists a special value of $\omega r_c/c$ (or, equivalently, of ε_0) for which the derivative $\alpha'_n(k_z)$ becomes zero. This means that the corresponding point is a higher-order pole of the integrand in (5.1). One of the possible ways to regularize this singularity is to include the imaginary part of the permittivity $\varepsilon_0(\omega)$. Note that this kind of problem does not appear in the problem of radiation from a charge circulating around a cylinder, discussed in [31,32]. The
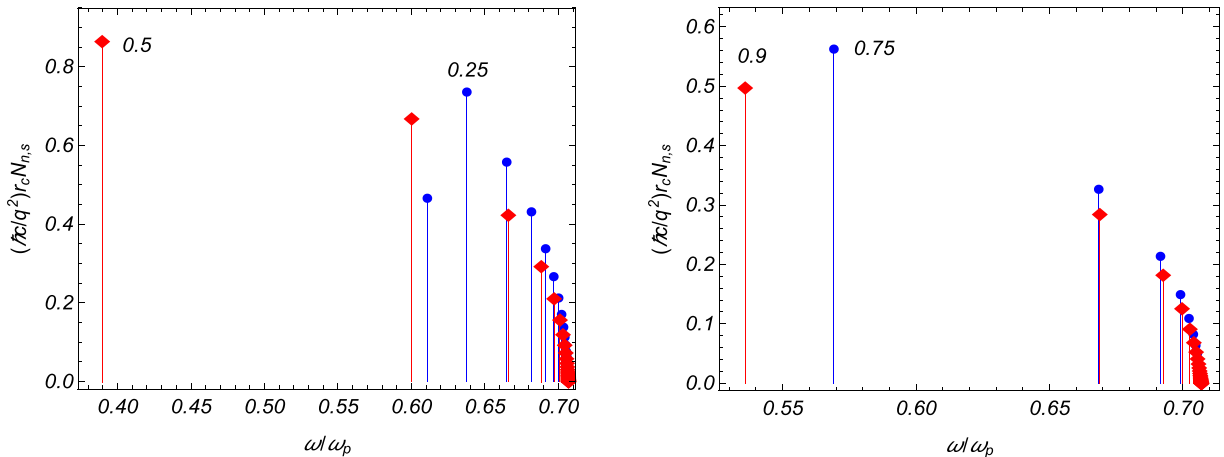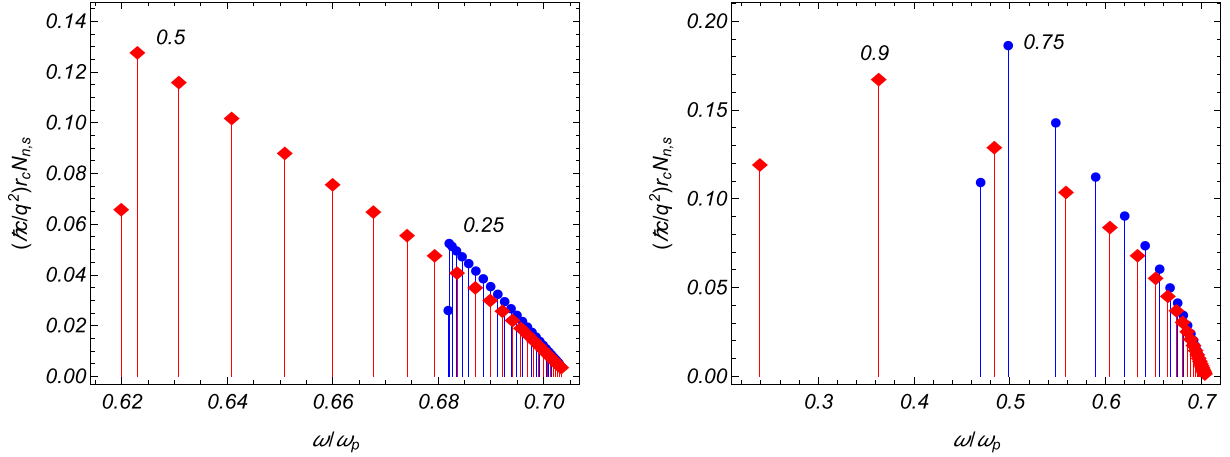

FIG. 10. The number of the radiated quanta in the form of surface polaritons, as a function of the frequency, for different values of $n \in [0, 20]$ (for the values of the parameters, see the text).

FIG. 11. The same as in Fig. 10, for $\omega_p r_c/c = 5$.

reason is that in the latter problem, for a given n, the radiation frequency $\nu = n/T$, with T being the charge rotation period and k_z are independent variables. As a consequence of this, for evaluation of $\alpha'_n(k_z)$, the derivative $\partial_\omega \varepsilon_0(\omega)$ is not required and a given value of ε_0 determines both the eigenvalues of k_z and the radiation intensity.

Given the importance of dispersion in discussing the emission of surface polaritons, in Fig. 10, for the dispersion law (6.6) with $\varepsilon_\infty = 1$, $\gamma = 0$, and for $\varepsilon_1 = 1$, the number of the radiated quanta for surface polaritons is presented as a function of the frequency (in units of the plasma frequency) $\omega/\omega_p = \omega_{n,s}/\omega_p$ for $n \in [0, 20]$. In the numerical evaluation, we have taken $r_0/r_c = 1.05$ and $\omega_p r_c/c = 1$. The circles and diamonds in the plot correspond to $v/c = 0.25$ and $v/c = 0.5$ on the left panel and to $v/c = 0.75$ and $v/c = 0.9$ on the right panel. Note that the eigenfrequencies increase with increasing n, $\omega_{n,s} < \omega_{n+1,s}$. The same data for $\omega_p r_c/c = 5$ are presented in Fig. 11. As already concluded from the asymptotic analysis, for large n the radiation frequencies tend to the value $\omega_p/\sqrt{\varepsilon_\infty + \varepsilon_1}$ ($= \omega_p/\sqrt{2}$ for the examples in Figs. 10 and 11). The spectral range of the radiated surface polaritons becomes narrower with decreasing v/c.

In the discussion above, we have considered the radiation from a single point charge. The corresponding results for the spectral density of the radiation intensity can be generalized for a bunch containing N_q particles. Let us consider a simple case of the bunch with transverse beam size that is smaller than the radiation wavelength. The z component of the current density is presented as $j_3^{(b)}(t, \mathbf{r}) = \sum_{m=1}^{N_q} j_{m3}(t, \mathbf{r})$, where the expression for the current density $j_{m3}(t, \mathbf{r})$ for the mth particle in the bunch is obtained from (2.2) by the replacement $z \to z - z_m$, with z_m being the z coordinate of the mth particle at the initial moment $t = 0$. The expressions for the Fourier components of the fields are obtained from the corresponding formulas given above for a single charge by adding the factor $\sum_{m=1}^{N_q} e^{-ik_z z_m}$, with $k_z = \omega/v$. In the expression for the radiation intensity, the factor $\left| \sum_{m=1}^{N_q} e^{-ik_z z_m} \right|^2$ will appear. The double sum in this modulus squared, $\sum_{m,m'=1}^{N_q}$, is decomposed into the incoherent contribution with $m' = m$ and the remaining coherent contribution. Introducing the longitudinal distribution function of the bunch $f(z)$ in accordance with

$\sum_{m=1}^{N_q} \int_{-\infty}^{+\infty} dz \, \delta(z - z_n) e^{-ik_z z} = N_q \int_{-\infty}^{+\infty} dz \, f(z) e^{-ik_z z}$, we see that the radiation intensity from a bunch is obtained from the formulas for a single charge by adding an additional geometrical factor,

$$N_q[1 + (N_q - 1)|g(k_z)|^2], \qquad (6.15)$$

where $g(k_z) = \int_{-\infty}^{+\infty} dz \, f(z) e^{-ik_z z}$. For a Gaussian bunch, one has $f(z) = e^{-z^2/2\sigma_z^2}/(\sqrt{2\pi}\sigma_z)$ and $|g(k_z)|^2 = \exp(-k_z^2 \sigma_z^2)$, with σ_z being the rms bunch length. The second term in the squared brackets of (6.15) presents the contribution of the coherent effects in the radiation intensity.

In the discussion above, we have assumed that the waveguide has infinite length along its axis. This allowed one to provide an exact solution for the problem under consideration. In fact, the majority of the papers cited above, that consider the radiation in waveguides, used this approximation. The results for the fields given above will approximate the features for a dielectric cylinder with the length L_c under the conditions $r, r_0, \lambda_r \ll L_c$, with λ_r being the radiation wavelength. For a finite cylinder, in addition to the radiations discussed above, there will be diffraction radiation at the ends. Another interesting effect at the termination of the waveguide corresponds to the transformation of guided modes and surface polaritons to free electromagnetic fields propagating in the surrounding medium.

VII. CONCLUSION

We have investigated the radiation emitted by a charge uniformly moving outside a dielectric cylinder, parallel to its axis. The electric and magnetic fields are found for general cases of dielectric permittivities of the cylinder and surrounding medium. First we have investigated the spectral density for the CR intensity in the exterior medium by evaluating the energy flux at large distances from the charge. The spectral density is given by (3.4) with functions $f_n^{(p)}$ from (2.11). It has been shown that the influence of the cylinder on the CR is essentially different in the cases $\varepsilon_0 < \varepsilon_1$ and $\varepsilon_0 > \varepsilon_1$. The characteristic feature in the first case is presented in Fig. 2 with relatively small oscillations of the spectral density of the radiation intensity around the value corresponding to the

radiation in a homogeneous medium. For wavelengths much smaller than the cylinder diameter, the oscillations enter into a quasiperiodic regime. These oscillations result from the interference of the direct CR, the CR reflected from the cylinder, and also the CR formed inside the cylinder if the corresponding Cherenkov condition is obeyed. In the case $\varepsilon_0 > \varepsilon_1$, strong narrow peaks may appear in the spectral distribution of the radiation intensity. We have specified the conditions for the presence of those peaks. They come from the terms of the series in (3.4) with large values of n and are closely related to the eigenvalue equation for the dielectric cylinder. Equation (3.13) that determines the spectral locations of the peaks is obtained form the eigenvalue equation $\alpha_n = 0$, ignoring the exponentially small terms of the order of $|J_n(\lambda_1 r_c)|/Y_n(\lambda_1 r_c)$. Under the Cherenkov condition with the dielectric permittivity of the surrounding medium, the eigenvalue equation has no solutions and the radiation modes corresponding to the strong peaks could be called "quasimodes" of the dielectric cylinder. The radiation on these types of modes may also appear in the spectral range where $\varepsilon_0 < -\varepsilon_1$. We have analytically estimated the heights and widths of the peaks by using the asymptotic expressions for the cylinder functions for large arguments.

If the Cherenkov condition for the exterior medium is not satisfied, depending on the spectral range, two types of radiations may appear propagating inside the cylindrical waveguide. They have a discrete spectrum determined by the dispersion relation $\alpha_n = 0$. The corresponding fields exponentially decay as functions of the distance from the cylinder surface and they correspond to guided modes and to surface polaritons. For guided modes, $\lambda_0^2 > 0$ and the Cherenkov condition is satisfied for the dielectric permittivity of the cylinder. For those modes, the radial dependence of the fields is expressed in terms of the Bessel function $J_n(\lambda_0 r)$ and the radiation intensity is given by (5.9). The lower threshold for the guided modes' frequency increases with increasing n and the radiation frequency range is determined by (5.10).

Unlike the guided modes, there is no velocity threshold for the emission of surface polaritons. They are radiated in the spectral range where the dielectric permittivities of the cylinder and of the surrounding medium have opposite signs. The corresponding radial dependence of the radiation fields inside the cylinder is described by the Bessel modified function $I_n(|\lambda_0|r)$ and the radiation intensity on a given frequency is expressed as (6.11). The dispersion for surface polaritons is qualitatively different for the modes with $n = 0$ and $n \geqslant 1$. For $n = 0$, there is an upper threshold for the values of the permittivity ε_0 [given by (6.2)]: the eigenvalue equation has a single root in the region $\varepsilon_0 < \varepsilon_0^{(\infty)}$ and there are no surface modes in the range $\varepsilon_0 > \varepsilon_0^{(\infty)}$. In the case $n \geqslant 1$, a single or two surface modes exist in the finite range $\varepsilon_0^{(m)} \leqslant \varepsilon_0 < -\varepsilon_1$, with the lower threshold $\varepsilon_0^{(m)}$ depending on n and v/c. In the nonrelativistic limit, $\varepsilon_0^{(m)}$ tends to $-\varepsilon_1$ and the surface modes are present in the narrow range for ε_0 with the length of the order of β_1^2. For illustration of the general results, as an example of dispersion for dielectric permittivity of the cylinder, we have considered a Drude-type model. In the limiting regions of the dimensionless parameter $\omega_p r_c/v$, the frequencies of the surface modes are estimated by (6.7)–(6.9). The radiation intensities for surface polaritons in those regions are approximated by (6.13) and (6.14). The spectral range of the generated surface polaritons becomes narrower with decreasing v/c. Having the fields and radiation intensity for a single charge, one can obtain the corresponding result for a bunch of particles. In the simple case of the bunch with small transverse size, the effect of the bunch appears in the form of the geometrical factor (6.15) determined by the bunch longitudinal form factor.

ACKNOWLEDGMENT

---

[1] J. V. Jelly, *Cerenkov Radiation and Its Applications* (Pergamon, London, 1958); V. P. Zrelov, *Vavilov-Cherenkov Radiation in High-Energy Physics* (Israel Program for Scientific Translations, Jerusalem, 1970); G. N. Afanasief, *Vavilov-Cherenkov and Synchrotron Radiation* (Springer, Netherlands, 2004).

[2] B. M. Bolotovskii, Theory of the vavilov-cherenkov effect, Usp. Fiz. Nauk **62**, 201 (1957); Theory of the Vavilov-Cherenkov effect (III), **75**, 295 (1961) [Sov. Phys. Usp. **4**, 781 (1961)].

[3] R. Marqués, F. Martín, and M. Sorolla, *Metamaterials with Negative Parameters: Theory, Design, and Microwave Applications* (Wiley, Hoboken, NJ, 2008).

[4] V. G. Veselago, The electrodynamics of substances with simultaneously negative values of ϵ and μ, Sov. Phys. Usp. **10**, 509 (1968).

[5] H. Chen and M. Chen, Flipping photons backward: reversed Cherenkov radiation, Mater. Today **14**, 34 (2011); Z. Su, B. Xiong, Y. Xu, Z. Cai, J. Yin, R. Peng, and Y. Liu, Manipulating cherenkov radiation and smithpurcell radiation by artificial structures, Adv. Opt. Mater. **7**, 1801666 (2019).

[6] J. Lu, T. M. Grzegorczyk, Y. Zhang, J. Pacheco Jr, B.-I. Wu, and J. A. Kong, Cerenkov radiation in materials with negative permittivity and permeability, Opt. Express **11**, 723 (2003); S. Antipov, L. Spentzouris, W. Liu, W. Gai, and J. G. Power, Wakefield generation in metamaterial-loaded waveguides, J. Appl. Phys. **102**, 034906 (2007); S. Antipov, L. Spentzouris, W. Gai, M. Conde, F. Franchini, R. Konecny, W. Liu, J. G. Power, Z. Yusof, and C. Jing, Observation of wakefield generation in left-handed band of metamaterialloaded waveguide, *ibid.* **104**, 014901 (2008); S. Xi, H. Chen, T. Jiang, L. Ran, J. Huangfu, B.-I. Wu, J. A. Kong, and M. Chen, Experimental Verification of Reversed Cherenkov Radiation in Left-Handed Metamaterial, Phys. Rev. Lett. **103**, 194801 (2009); J.-K. So, J.-H. Won, M. A. Sattorov, S.-H. Bak, K.-H. Jang, G.-S. Park, D. S. Kim, and F. J. Garcia-Vidal, Cerenkov Radiation in Metallic Metamaterials, Appl. Phys. Lett. **97**, 151107 (2010); V. V. Vorobev and A. V. Tyukhtin, Nondivergent Cherenkov Radiation in a Wire Metamaterial, Phys. Rev. Lett. **108**, 184801 (2012).

[7] D. E. Fernandes, S. I. Maslovski, and M. G. Silveirinha, Cherenkov emission in a nanowire material, Phys. Rev. B **85**, 155107 (2012); S. Smirnov, Cherenkov sound on a surface of a topological insulator, *ibid.* **88**, 205301 (2013); X. Lu, M. A. Shapiro, and R. J. Temkin, Modeling of the interaction of a volumetric metallic metamaterial structure with a relativistic electron beam, Phys. Rev. Spec. Top. Accel. Beams **18**, 081303 (2015); J. S. Hummelt, X. Lu, H. Xu, I. Mastovsky, M. A. Shapiro, and R. J. Temkin, Coherent Cherenkov-Cyclotron Radiation Excited by an Electron Beam in a Metamaterial Waveguide, Phys. Rev. Lett. **117**, 237701 (2016); Z. Duan, X. Tang, Z. Wang, Y. Zhang, X. Chen, M. Chen, and Y. Gong, Observation of the reversed Cherenkov radiation, Nat. Commun. **8**, 14901 (2017); X. Lu, J. C. Stephens, I. Mastovsky, M. A. Shapiro, and R. J. Temkin, Linear theory of instabilities generated by an electron beam in a metamaterial-loaded waveguide, Phys. Plasmas **25**, 023102 (2018); X. Lu, M. A. Shapiro, I. Mastovsky, R. J. Temkin, M. Conde, J. G. Power, J. Shao, E. E. Wisniewski, and Ch. Jing, Coherent High-Power RF Wakefield Generation by Electron Bunch Trains in a Metamaterial Structure, Phys. Rev. Lett. **122**, 014801 (2019); O. J. Franca, L. F. Urrutia, and O. Rodríguez-Tzompantzi, Reversed electromagnetic Vasilov-Cerenkov radiation in naturally existing magnetoelectric media, Phys. Rev. D **99**, 116020 (2019).

[8] F. J. García de Abajo and A. Howie, Retarded field calculation of electron energy loss in inhomogeneous dielectrics, Phys. Rev. B **65**, 115418 (2002); F. J. García de Abajo, A. Rivacoba, N. Zabala, and N. Yamamoto, Boundary effects in Cherenkov radiation, *ibid.* **69**, 155420 (2004); F. J. García de Abajo, Optical excitations in electron microscopy, Rev. Mod. Phys. **82**, 209 (2010); S. N. Galyamin and A. V. Tyukhtin, Electromagnetic Field in Dielectric Concentrator for Cherenkov Radiation, Phys. Rev. Lett. **113**, 064802 (2014); E. S. Belonogaya, S. N. Galyamin, and A. V. Tyukhtin, Short-wavelength radiation of a charge moving in the presence of a dielectric prism, J. Opt. Soc. Am. B **32**, 649 (2015); A. Tyukhtin, V. Vorobev, E. Belonogaya, and S. Galyamin, Cherenkov radiation of a charge flying through the "inverted" conical target, JINST **13**, C02033 (2018); A. P. Potylitsyn and S. Yu. Gogolev, Vavilov-Cherenkov Radiation in an Inclined Dielectric Plate and Violation of Azimuthal Symmetry, Phys. Part. Nuclei Lett. **16**, 127 (2019); A. V. Tyukhtin, S. N. Galyamin, and V. V. Vorobev, Peculiarities of Cherenkov radiation from a charge moving through a dielectric cone, Phys. Rev. A **99**, 023810 (2019).

[9] J. E. Walsh, T. C. Marshall, and S. P. Shlesinger, Generation of coherent Cerenkov radiation with an intense relativistic electron beam, Phys. Fluid. **20**, 709 (1977); N. Zabala, A. Rivacoba, and P. M. Echenique, Energy loss of electrons travelling through cylindrical holes, Surf. Sci. **209**, 465 (1989); K. L. Felch, K. O. Busby, R. W. Layman, D. Kapilow, and J. E. Walsh, Cerenkov Radiation in Dielectric-Lined Waveguides, Appl. Phys. Lett. **38**, 601 (1998); P. Schoessow, M. E. Conde, W. Gai, R. Konecny, J. Power, and J. Simpson, High power radio frequency generation by relativistic beams in dielectric structures, J. Appl. Phys. **84**, 663 (1998); Z. Duan, B.-I. Wu, J. Lu, J. A. Kong, and M. Chen, Reversed Cherenkov radiation in a waveguide filled with anisotropic double-negative metamaterials, *ibid.* **104**, 063303 (2008); G. Adamo, K. F. MacDonald, Y. H. Fu, C.-M. Wang, D. P. Tsai, F. J. García de Abajo, and N. I. Zheludev, Light Well: A Tunable Free-Electron Light Source on a Chip,

Phys. Rev. Lett. **103**, 113901 (2009); L. S. Grigoryan, H. F. Khachatryan, and S. R. Arzumanyan, Self-amplified Cherenkov radiation from relativistic particles in layered dielectric-filled waveguide, Nuovo Cim. C **34**, 317 (2011); I. V. Konoplev, A. J. MacLachlan, C. W. Robertson, A. W. Cross, and A. D. R. Phelps, Cylindrical periodic surface lattice as a metadielectric: Concept of a surface-field Cherenkov source of coherent radiation, Phys. Rev. A **84**, 013826 (2011); S. Liu, M. Hu, Y. Zhang, W. Liu, P. Zhang, and J. Zhou, Theoretical investigation of a tunable free-electron light source, Phys. Rev. E **83**, 066609 (2011); L. S. Grigoryan, A. R. Mkrtchyan, H. F. Khachatryan, S. R. Arzumanyan, and W. Wagner, Self-amplified Cherenkov radiation from a relativistic electron in a waveguide partially filled with a laminated material, J. Phys. Conf. Ser. **357**, 012004 (2012).

[10] A. M. Cook, R. Tikhoplav, S. Y. Tochitsky, G. Travish, O. B. Williams, and J. B. Rosenzweig, Observation of Narrow-Band Terahertz Coherent Cherenkov Radiation from a Cylindrical Dielectric-Lined Waveguide, Phys. Rev. Lett. **103**, 095003 (2009); G. Andonian, O. Williams, X. Wei, and P. Niknejadi, E. Hemsing *et al.*, Resonant Excitation of Coherent Cerenkov Radiation in Dielectric Lined Waveguides, Appl. Phys. Lett. **98**, 202901 (2011).

[11] S. N. Galyamin, A. V. Tyukhtin, S. Antipov, and S. S. Baturin, Terahertz radiation from an ultra-relativistic charge exiting the open end of a waveguide with a dielectric layer, Opt. Express **22**, 8902 (2014); T. Yu. Alekhina and A. V. Tyukhtin, Cherenkov-transition radiation in a waveguide with a dielectric-vacuum boundary, Phys. Rev. Spec. Top. Accel. Beams **15**, 091302 (2012); A. Smirnov, Characterization of coherent Cherenkov radiation source, Nucl. Instrum. Methods Phys. Res., Sect. A **771**, 147 (2015); V. Bleko, P. Karataev, A. Konkov, K. Kruchinin, G. Naumenko, A. Potylitsyn, and T. Vaughan, Coherent cherenkov radiation as an intense THz source, J. Phys.: Conf. Ser. **732**, 012006 (2016); S. N. Galyamin, A. V. Tyukhtin, and V. V. Vorobev, Radiation from open ended waveguide with dielectric loading, Nucl. Instrum. Methods Phys. Res., Sect. B **402**, 144 (2017); S. N. Galyamin, A. V. Tyukhtin, V. V. Vorobev, A. A. Grigoreva, and A. S. Aryshev, Cherenkov radiation of a charge exiting open-ended waveguide with dielectric filling, Phys. Rev. Spec. Top. Accel. Beams **22**, 012801 (2019); S. Jiang, W. Li, Z. He, R. Huang, Q. Jia, L. Wang, and Y. Lu, High power THz coherent Cherenkov radiation based on a separated dielectric loaded waveguide, Nucl. Instrum. Methods Phys. Res., Sect. A **923**, 45 (2019); A. R. Mkrtchyan, L. S. Grigoryan, A. A. Saharian, A. H. Mkrtchyan, H. F. Khachatryan, and V. K. Kotanjyan, Self-amplification of radiation from an electron bunch inside a waveguide filled with periodic medium, JINST **15**, C06019 (2020).

[12] Yu. O. Averkov and V. M. Yakovenko, Cherenkov radiation by an electron bunch that moves in a vacuum above a left-handed material, Phys. Rev. B **72**, 205110 (2005); M. I. Bakunov, M. V. Tsarev, and M. Hangyo, Cherenkov emission of terahertz surface plasmon polaritons from a superluminal optical spot on a structured metal surface, Opt. Express **17**, 9323 (2009); I. V. Konoplev, L. Fisher, A. W. Cross, A. D. R. Phelps, K. Ronald, and C. W. Robertson, Surface Wave Cherenkov Maser Based on a Periodic Lattice, Appl. Phys. Lett. **96**, 261101 (2010); V. S. Zuev, A. M. Leontovich, and V. V. Lidsky,

Cherenkov Excitation of Surface Waves, JETP Lett. **91**, 115 (2010); Cherenkov-like mechanism of surface waves excitation, Opt. Spectrosc. **110**, 411 (2011); J. Tao, Q. J. Wang, J. Zhang, and Y. Luo, Reverse surface-polariton Cherenkov radiation, Sci. Rep. **6**, 30704 (2016); P. Kumar, R. Kumar, and S. K. Rajouria, Cherenkov terahertz surface plasmon excitation by an electron beam over an ultrathin metal film, J. Appl. Phys. **120**, 223101 (2016).

[13] S. Liu, P. Zhang, W. Liu, S. Gong, R. Zhong, Y. Zhang, and M. Hu, Surface Polariton Cherenkov Light Radiation Source, Phys. Rev. Lett. **109**, 153902 (2012); T. Zhao, R. Zhong, M. Hu, X. Chen, P. Zhang, S. Gong, and S. Liu, Cherenkov Radiation Via Surface Plasmon Polaritons Excitation by an Electron Beam in a Layered Metal-Dielectric Structure, Eur. Phys. J. D **69**, 120 (2015); T. Zhao, M. Hu, R. Zhong, S. Gong, C. Zhang, and S. Liu, Cherenkov Terahertz Radiation from Graphene Surface Plasmon Polaritons Excited by an Electron Beam, Appl. Phys. Lett. **110**, 231102 (2017); C. Yu and S. Liu, Quantum Theory of Surface Polariton Cherenkov Light Radiation Source and Its Fluctuation, *ibid.* **114**, 181106 (2019).

[14] N. Zabala, E. Ogando, A. Rivacoba, and F. J. García de Abajo, Inelastic scattering of fast electrons in nanowires: A dielectric formalism approach, Phys. Rev. B **64**, 205410 (2001); Y.-N. Wang and Z. L. Mišković, Energy loss of charged particles moving in cylindrical tubules, Phys. Rev. A **66**, 042904 (2002).

[15] L. Sh. Grigoryan, A. S. Kotanjyan, and A. A. Saharian, Green function of an electromagnetic field in cylindrically symmetric inhomogeneous medium, Izv. Nats. Akad. Nauk Arm., Fiz. **30**, 239 (1995) (J. Contemp. Phys.).

[16] A. S. Kotanjyan, H. F. Khachatryan, A. V. Petrosyan, and A. A. Saharian, On the features of radiation from charged particle rotating around a dielectric cylinder, Izv. Nats. Akad. Nauk Arm., Fiz. **35**, 115 (2000) (J. Contemp. Phys.); A. S. Kotanjyan and A. A. Saharian, Radiation from an electron rotating inside a dielectric cylinder, *ibid.* **37**, 135 (2002) (J. Contemp. Phys.); A. S. Kotanjyan, Radiation from a charged particle rotating inside a dielectric cylinder, Nucl. Instrum. Methods Phys. Res., Sect. B **201**, 3 (2003); A. A. Saharian, A. S. Kotanjyan, L. Sh. Grigoryan, H. F. Khachatryan, and V. Kh. Kotanjyan, Synchrotron radiation from a charge circulating around a cylinder with negative permittivity, Int. J. Mod. Phys. B **34**, 2050065 (2020).

[17] A. A. Saharian and A. S. Kotanjyan, Synchrotron radiation from a charge moving along a helical orbit inside a dielectric cylinder, J. Phys. A: Math. Gen. **38**, 4275 (2005); S. R. Arzumanyan, L. Sh. Grigoryan, H. F. Khachatryan, A. S. Kotanjyan, and A. A. Saharian, On features of the radiation from an electron moving along a helix inside a cylindrical hole in a homogeneous dielectric, Nucl. Instrum. Methods Phys. Res., Sect. B **266**, 3703 (2008); A. A. Saharian and A. S. Kotanjyan, Synchrotron radiation from a charge moving along a helix around a dielectric cylinder, J. Phys. A: Math. Gen. **42**, 135402 (2009); A. S. Kotanjyan and A. A. Saharian, Undulator radiation inside a dielectric waveguide, Nucl. Instrum. Methods Phys. Res., Sect. B **309**, 177 (2013).

[18] *Handbook of Mathematical Functions*, edited by M. Abramowitz and I. A. Stegun (Dover, New York, 1972).

[19] M. V. Berry, Attenuation and focusing of electromagnetic surface waves rounding gentle bends, J. Phys. A **8**, 1952 (1975); Surface waves with high angular momentum: leakage from

remote caustics, and tightly coiled streamlines, Eur. J. Phys. **39**, 045807 (2018).

[20] L. Sh. Grigoryan, H. F. Khachatryan, S. R. Arzumanyan, and M. L. Grigoryan, High power Cherenkov radiation from a relativistic particle rotating around a dielectric ball, Nucl. Instrum. Methods Phys. Res., Sect. B **252**, 50 (2006); S. R. Arzumanyan, L. Sh. Grigoryan, H. F. Khachatryan, and M. L. Grigoryan, The features of synchrotron radiation from a relativistic particle rotating inside a spherical cavity, *ibid.* **266**, 3715 (2008); L. Sh. Grigoryan, A. A. Saharian, H. F. Khachatryan, M. L. Grigoryan, A. V. Sargsyan, and T. A. Petrosyan, Angular distribution of high power radiation from a charge rotating around a dielectric ball, JINST **15**, C04035 (2020).

[21] K. G. Dedrick, The influence of multiple scattering on the angular width of cerenkov radiation, Phys. Rev. **87**, 891 (1952); V. M. Grichine, Radiation of multiple-scattered charged particle, Nucl. Instrum. Methods Phys. Res., Sect. A **563**, 364 (2006); Y. Takabayashi, E. I. Fiks, and Yu. L. Pivovarov, First studies of 500-nm Cherenkov radiation from 255-MeV electrons in a diamond crystal, Phys. Lett. A **379**, 1032 (2015); J. Zheng, Angular width of the Cherenkov radiation with inclusion of multiple scattering, Phys. Plasmas **23**, 063117 (2016); B. A. Alekseeva, A. V. Vukolova, A. P. Potylitsyna, and M. V. Shevelev, Measuring Electron Beam Divergence with Cherenkov Light, Phys. Part. Nuclei Lett. **17**, 27 (2020).

[22] P. A. Zyla *et al.* (Particle Data Group), Review of particle physics, Prog. Theor. Expt. Phys. **2020**, 083C01 (2020).

[23] V. L. Ginzburg, *Applications of Electrodynamics in Theoretical Physics and Astrophysics* (Gordon and Breach, London, 1989).

[24] E. Esarey, C. B. Schroeder, and W. P. Leemans, Physics of laser-driven plasma-based electron accelerators, Rev. Mod. Phys. **81**, 1229 (2009); C. Jing, Dielectric wakefield accelerators, Rev. Accel. Sci. Technol. **09**, 127 (2016); E. Gschwendtner and P. Muggli, Plasma wakefield accelerators, Nat. Rev. Phys. **1**, 246 (2019); J. Ju, K. Svensson, H. Ferrari, A. Döpp, G. Genoud *et al.*, Study of electron acceleration and x-ray radiation as a function of plasma density in capillary-guided laser wakefield accelerators, Phys. Plasmas **20**, 083106 (2013).

[25] M. C. Thompson, H. Badakov, A. M. Cook, J. B. Rosenzweig, R. Tikhoplav *et al.*, Breakdown Limits on Gigavolt-Per-Meter Electron-Beam-Driven Wakefields in Dielectric Structures, Phys. Rev. Lett. **100**, 214801 (2008).

[26] B. D. O'Shea, G. Andonian, S. K. Barber, K. L. Fitzmorris, S. Hakimi *et al.*, Observation of acceleration and deceleration in gigaelectron-volt-per-metre gradient dielectric wakefield accelerators, Nat. Commun. **7**, 12763 (2016).

[27] J. D. Jackson, *Classical Electrodynamics* (Wiley, New York, 1999).

[28] *Surface Polaritons: Electromagnetic Waves at Surfaces and Interfaces*, edited by V. M. Agranovich and D. L. Mills (North-Holland, Amsterdam, 1982); S. A. Maier, *Plasmonics: Fundamentals and Applications* (Springer, New York, 2007); M. I. Stockman *et al.*, Roadmap on plasmonics, Roadmap on plasmonics, J. Optics **20**, 043001 (2018).

[29] P. R. West, S. Ishii, G. V. Naik, N. K. Emani, V. M. Shalaev, and A. Boltasseva, Searching for better plasmonic materials, Laser Photon. Rev. **4**, 795 (2010); N. C. Lindquist, P. Nagpal, K. M. McPeak, D. J. Norris, and S.-H. Oh, Engineering metallic nanostructures for

plasmonics and nanophotonics, Rep. Prog. Phys. **75**, 036501 (2012).

[30] X. Yao, X. Kou, and J. Qiu, Nano-Al_2O_3/PANI composites with high negative permittivity, Org. Electron, Org. Electron. **39**, 133 (2016); K. Sun, R. Fan, Y. Yin, J. Guo, X. Li, Y. Lei, L. An, C. Cheng, and Z. Guo, Tunable negative permittivity with fano-like resonance and magnetic property in percolative silver/yittrium iron garnet nanocomposites, J. Phys. Chem. C **121**, 7564 (2017).

[31] J. C. Ashley and L. C. Emerson, Dispersion relations for non-radiative surface plasmons on cylinders, Surf. Sci. **41**, 615 (1974); H. Khosravi, D. R. Tilley, and R. Loudon, Surface polaritons in cylindrical optical fibers, J. Opt. Soc. Am. A **8**, 112 (1991).

[32] A. S. Kotanjyan, A. R. Mkrtchyan, A. A. Saharian, and V. Kh. Kotanjyan, Generation of surface polaritons in dielectric cylindrical waveguides, Phys. Rev. Spec. Top. Accel. Beams **22**, 040701 (2019).